

ARTICLE

STING controls energy stress-induced autophagy and energy metabolism via STX17

Yueguang Rong^{2*}, Shen Zhang^{1*}, Nilay Nandi^{3*}, Zhe Wu^{2*}, Linsen Li¹, Yang Liu^{4,5}, Yuehan Wei⁶, Yuan Zhao², Weigang Yuan², Chuchu Zhou², Guanghua Xiao⁷, Beth Levine^{4,5}, Nan Yan⁸, Shan Mou⁶, Liufu Deng⁹, Zaiming Tang¹, Xiaoxia Liu¹, Helmut Kramer³, and Qing Zhong¹

The stimulator of interferon genes (STING) plays a critical role in innate immunity. Emerging evidence suggests that STING is important for DNA or cGAMP-induced non-canonical autophagy, which is independent of a large part of canonical autophagy machineries. Here, we report that, in the absence of STING, energy stress-induced autophagy is upregulated rather than downregulated. Depletion of STING in *Drosophila* fat cells enhances basal- and starvation-induced autophagic flux. During acute exercise, STING knockout mice show increased autophagy flux, exercise endurance, and altered glucose metabolism. Mechanistically, these observations could be explained by the STING–STX17 interaction. STING physically interacts with STX17, a SNARE that is essential for autophagosome biogenesis and autophagosome–lysosome fusion. Energy crisis and TBK1-mediated phosphorylation both disrupt the STING–STX17 interaction, allow different pools of STX17 to translocate to phagophores and mature autophagosomes, and promote autophagic flux. Taken together, we demonstrate a heretofore unexpected function of STING in energy stress-induced autophagy through spatial regulation of autophagic SNARE STX17.

Introduction

The stimulator of interferon genes (STING) is an ER protein with four transmembrane domains and a long cytoplasmic domain at its carboxyl terminus that binds ligands and signals downstream to induce IFN and other cytokine genes (Cai et al., 2014; Ishikawa and Barber, 2008; Jin et al., 2008; Sun et al., 2009; Zhong et al., 2008). Cyclic dinucleotide ligands such as cGAMP, which can be destabilized by pathogen-derived poxin (Eaglesham et al., 2019), bind STING and promote the dimerization and translocation of STING from the ER, in a sequential manner, to ERGIC, Golgi, and finally to endolysosomes (Burdette et al., 2011; Chu et al., 2021; Dobbs et al., 2015; Ishikawa et al., 2009; Saitoh et al., 2009; Sun et al., 2013; Woodward et al., 2010; Wu et al., 2013). Cytosolic mitochondrial DNA (mtDNA) released by mitophagy defects activates cGAS–STING pathway and leads to inflammation, which is completely rescued by the concurrent loss of STING (Sliter et al., 2018). cGAS–STING trafficking and activation are negatively regulated by autophagy or autophagy proteins ATG9 and Beclin1 (Chen et al., 2016; Gkirtzimanaki et al., 2018; Levine

et al., 2011; Liang et al., 2014; Saitoh et al., 2009), while the recognition of bacterial DNA by the STING-dependent cytosolic pathway is important for autophagic recognition of *Mycobacterium tuberculosis* (Watson et al., 2012). STING senses c-di-AMP and then drives ER-phagy and IFN production to relieve the ER stress, thereby protecting cells from infection-induced cell death (Moretti et al., 2017). Recently, it is reported that STING activation induces non-canonical autophagy, independently of ULK1, Beclin1, and ATG9a (Gui et al., 2019; Liu et al., 2019). Also, the STING-dependent downstream TANK-binding kinase 1 (TBK1) phosphorylates STX17 in autophagy initiation (Kumar et al., 2019). All these emerging pieces of evidence illustrate a crucial role of STING in DNA or cGAMP-induced non-canonical autophagy. However, how STING regulates energy crisis-induced autophagy remains largely unknown.

The process of autophagy includes autophagosome biogenesis, autophagosome–lysosome fusion, autophagic cargos degradation in autolysosomes, and the recycling of autophagic

¹Key Laboratory of Cell Differentiation and Apoptosis of Chinese Ministry of Education, Department of Pathophysiology, Shanghai Jiao Tong University School of Medicine, Shanghai, China; ²Department of Pathogen Biology, School of Basic Medicine, Huazhong University of Science and Technology, Wuhan, China; ³Department of Neuroscience and Department of Cell Biology, University of Texas Southwestern Medical Center, Dallas, TX; ⁴Center for Autophagy Research, Department of Internal Medicine, University of Texas Southwestern Medical Center, Dallas, TX; ⁵Howard Hughes Medical Institute, University of Texas Southwestern Medical Center, Dallas, TX; ⁶Department of Nephrology, Renji Hospital, Shanghai Jiao Tong University School of Medicine, Shanghai, China; ⁷Quantitative Biomedical Research Center, Department of Clinical Sciences, University of Texas Southwestern Medical Center, Dallas, TX; ⁸Department of Immunology, University of Texas Southwestern Medical Center, Dallas, TX; ⁹Department of Immunology and Microbiology, Shanghai Jiao Tong University School of Medicine, Shanghai, China.

Beth Levine died on June 16, 2020. *Y. Rong, S. Zhang, N. Nandi, and Z. Wu contributed equally to this paper. Correspondence to Qing Zhong: qingzhong@shsmu.edu.cn; Xiaoxia Liu: xxliu@shsmu.edu.cn; Yueguang Rong: rongyueguang@hust.edu.cn; Helmut Kramer: helmut.kramer@utsouthwestern.edu.

© 2022 Rong et al. This article is distributed under the terms of an Attribution–Noncommercial–Share Alike–No Mirror Sites license for the first six months after the publication date (see <http://www.rupress.org/terms/>). After six months it is available under a Creative Commons License (Attribution–Noncommercial–Share Alike 4.0 International license, as described at <https://creativecommons.org/licenses/by-nc-sa/4.0/>).

machinery or nutrient molecules (Levine and Kroemer, 2019; Mizushima, 2007). The cargo engulfed in autophagosome is delivered to lysosomes for degradation through autophagosome-lysosome membrane fusion. The membrane fusion is a highly conserved process driven by SNARE proteins (soluble N-ethylmaleimide-sensitive factor attachment protein receptors), where the SNARE domains of SNARE proteins zipper to form a parallel four α -helix bundle to complete the fusion. For autophagy in yeast, membrane fusion between autophagosomes and vacuoles is mediated by Ykt6 (R-SNARE) on autophagosomes, and Vam3 (Qa-SNARE), Vti1 (Qb-SNARE), and Vam7 (Qc-SNARE) on vacuoles (Bas et al., 2018; Gao et al., 2018). On the other hand, the SNAREs mediating autophagic membrane fusion in metazoan cells is more complicated. In mammalian cells, the first set of SNAREs to drive the autophagosome-lysosome fusion was identified by Mizushima et al. (2019), which is STX17 (Qa-SNARE) from autophagosomes, SNAP29 (Qb, Qc-SNARE) and VAMP8 (R-SNARE) from lysosomes. This set of SNARE complex was well proved to mediate fusion by in vitro reconstitution assay (Diao et al., 2015; Wang et al., 2016). Later, YKT6 (R-SNARE) was identified on autophagosome to mediate autophagosome-lysosome fusion along with SNAP29 and STX7 as a likely parallel fusion SNARE set in mammalian cells (Matsui et al., 2018; Mizushima et al., 2019), or identified on lysosome to act as a non-conventional SNARE to regulate STX17-dependent fusion in flies, where a fusion defect mutation of Ykt6 in the ionic zero-layer arginine (R) residue to glutamine (Q) does not abolish its function in autophagy (Takats et al., 2018).

STX17 is not only crucial for autophagosome-lysosome fusion in metazoan systems (Diao et al., 2015; Itakura et al., 2012; Jiang et al., 2014; Saleeb et al., 2019; Takats et al., 2013; Vats and Manjithaya, 2019) but is also important for autophagosome biogenesis (Hamasaki et al., 2013; Kumar et al., 2019; Kumar et al., 2021). MAM (mitochondria-associated ER membrane)-resident STX17 recruits ATG14 to initiate autophagosome formation (Hamasaki et al., 2013). TBK1 phosphorylated STX17 translocates to a hybrid PAS for autophagy initiation (Kumar et al., 2019; Kumar et al., 2021). In addition, different subcellular distribution of STX17 includes autophagosome/autolysosome, ER, Golgi, MAM, and mitochondria contributing to its autophagy regulatory functions (Arasaki et al., 2015; Itakura et al., 2012; Kumar et al., 2019; Sugo et al., 2018). However, it is not clear how autophagic-fusion involving STX17 is shuffled from which organelle and what is the trafficking regulation mechanism.

In this study, we found that STING negatively regulates energy stress-induced autophagy. Energy crisis disrupts STING-STX17 interaction, allowing STX17 to translocate to mature autophagosomes for fusion with lysosomes to promote autophagy flux. Besides, phosphorylation of STX17 at Ser202 affects its interaction with STING. The phosphorylation form of STX17 is not bound to STING and is mainly translocated to phagophores for autophagosome biogenesis. Furthermore, STING-regulated autophagy is crucial for energy metabolism. Taken together, we identified a new function of STING in energy stress-induced

autophagy distinct from its role in DNA or cGAMP induced non-canonical autophagy.

Results

STING negatively regulates energy stress-induced autophagy in *Drosophila*

We designed an experiment to examine the energy stress-induced autophagy activity in animals missing STING. STING is evolutionarily conserved in metazoa. Similar to mammalian STING, *Drosophila melanogaster* STING (dSTING) also translocates to perinuclear regions in response to cyclic dinucleotides stimulation (Goodman et al., 2013). One major difference is that dSTING lacks an extreme carboxyl terminus that is essential for its binding to TBK1 and for TBK1-IRF3 signaling in mammals, suggesting that its immune function is likely less active in flies (Goodman et al., 2013; Wu et al., 2014). Autophagy is evolutionarily conserved in *Drosophila* and plays a critical role in response to starvation in the fat body. Both basal and energy stress-induced autophagy activity was examined in *Drosophila* fat body depleted for dSTING by small interference RNA (RNAi). In *Drosophila* fat body with dSTING knocked down (Fig. 1 A), the number of ATG8a puncta in both fed and starved conditions dramatically decreased, compared with WT (wild-type) *Drosophila* fat body (Fig. 1, B-E). Atg8a reduction is not due to defective autophagosome formation since the overall number of ATG8a puncta in dSTING knock-down larvae upon chloroquine (CQ) treatment was unchanged compared with WT larvae in both fed and starved conditions (Fig. 1, B-E), suggesting that autophagic flux is likely enhanced in dSTING-deficient fat body cells. This phenomenon of increased autophagic flux upon STING depletion was further confirmed in STING knockout (KO) fat body (Fig. 1, F and G). We further dissected which steps of autophagy are affected by STING in *Drosophila* fat body. The lysosomes/autolysosomes labeled by LAMP-GFP were examined in WT and dSTING RNAi-depleted *Drosophila*. The number of puncta labeled by LAMP-GFP in dSTING knock-down fat bodies was significantly increased compared with WT flies (Fig. 1, H-J). The observation was further supported by the increased acidified organelle number indicated by LysoTracker, an acidotropic dye that marks acidified lysosomes and autolysosomes in dSTING-deficient flies (Fig. 1, K and L). Taken together, these observations suggest that both basal and energy stress-induced autophagy are activated rather than compromised in STING deficient *Drosophila* fat body cells, which is clearly different from the reported function of STING in DNA or cGAMP induced non-canonical autophagy.

Fusion between autophagosomes and lysosomes in *Drosophila* is driven by a SNARE protein complex comprising STX17-SNAP29-VAMP7 (Diao et al., 2015; Itakura et al., 2012; Takats et al., 2018; Takats et al., 2013), and we checked whether the increased autophagy flux upon STING KO is affected by the autophagic fusion SNARE STX17. The results showed that in both fed and starved conditions, the decreased Atg8a puncta in STING KO fat body cells can be reversed by STING

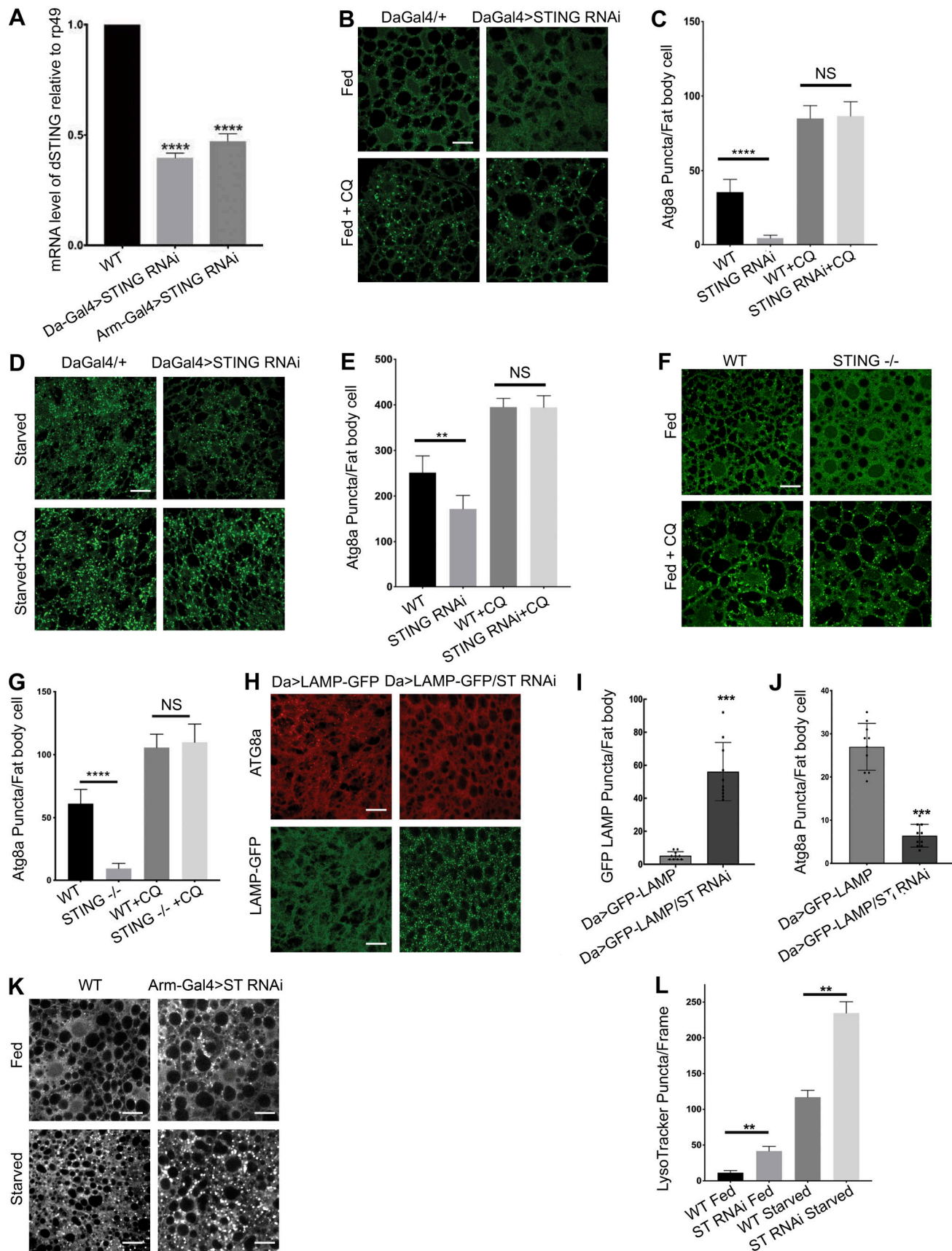


Figure 1. **STING negatively regulates canonical autophagy in *Drosophila* fat body.** (A) RT-qPCR was performed to measure the knockdown efficiency of STING RNAi driven by Da-Gal4 or Arm-Gal4 at 28°C. Each data point was repeated three times with independent samples and normalized with ribosomal *rp49*

gene as an internal control. **(B)** Micrographs of WT or dSTING siRNA knockdown fat bodies from 92–94-h-old size-matched larva fed with or without CQ (3 mg/ml) for 24 h. Projections of three sections' confocal micrographs encompassing six to eight cells stained for Atg8a. Scale bar, 20 μ m. **(C)** Quantification of Atg8a puncta in fat bodies averaged from five fed larvae from one representative experiment out of three repeats with or without CQ treatment. **, $P \leq 0.01$; NS, not significant. **(D)** Micrographs of WT or STING^{-/-} fat bodies from 92–94-h-old size-matched larva with or without CQ (3 mg/ml) for 24 h exposed to 20% sucrose solution to induce amino acid starvation. Projections of three sections of confocal micrographs encompassing six to eight cells stained for Atg8a. Scale bar, 20 μ m. **(E)** Quantification of Atg8a puncta in fat bodies averaged from five starved larvae from one representative experiment out of three repeats with or without CQ treatment. **, $P \leq 0.01$; NS, not significant. **(F)** Micrographs of WT or dSTING KO fat bodies from 92–94-h-old size-matched larva fed with or without CQ (3 mg/ml) for 24 h. Projections of three sections of confocal micrographs encompassing six to eight cells stained for Atg8a. Scale bar, 20 μ m. **(G)** Quantification of Atg8a puncta in fat bodies averaged from five fed larvae from one representative experiment out of three repeats with or without CQ treatment. ****, $P \leq 0.0001$; NS, not significant. **(H)** Micrographs of fat bodies from 92–94-h-old size-matched larva fed. Projections of three sections of confocal micrographs encompassing six to eight cells stained for Atg8a. GFP-LAMP was detected by GFP fluorescence in fixed tissue. Scale bar, 20 μ m. **(I)** Quantification of GFP-LAMP puncta in fat bodies averaged from five fed larvae from one representative experiment out of three repeats. ****, $P \leq 0.001$. **(J)** Quantification of ATG8a puncta in fat bodies averaged from five fed larvae from one representative experiment out of three repeats. ****, $P \leq 0.001$. **(K)** Micrographs of WT or dSTING knockdown fat bodies from 92–94-h-old size-matched larva fed or starved. Projections of three sections of confocal micrographs encompassing six to eight cells stained with LysoTracker. Scale bars are 20 μ m. **(L)** Quantification of LysoTracker puncta in fat bodies averaged from five fed or starved larvae from one representative experiment out of three repeats. **, $P \leq 0.01$. ST, STING.

overexpression or STX17 KO, while the total number of Atg8a puncta remained unchanged in CQ treated WT and STING KO fat body cells (Fig. 2, A–D). These indicated that in *Drosophila* the increased autophagy flux upon STING KO is likely through the regulation of STX17.

STING deficiency boosts exercise-induced autophagy in mice

Next, we asked if the function of STING in energy stress-induced autophagy is evolutionally conserved from *Drosophila* to mammals. We investigated whether STING modulates autophagy-regulated biological processes in STING-expressing tissues in mice. We found that STING is ubiquitously expressed in various mouse tissues, including skeletal muscles and brain, in addition to the known immune cells (Fig. 3 A). It is well reported that autophagy occurs in skeletal muscles with basal levels, and acute exercise can induce autophagy in skeletal muscle and promote muscle glucose metabolism (He et al., 2012). We therefore tested if STING deficiency enhances exercise-induced autophagy by crossing *Sting*^{-/-} mice to GFP-LC3 mice. As expected, the number of GFP-LC3 puncta is increased in muscles (EDL and thigh) after exercise (95 min running), but the total number of LC3 puncta is much less in muscles of *Sting*^{-/-} mice before and after exercise (Fig. 3, B–E). Reduction in LC3 puncta is due to increased autophagic degradation rather than attenuated autophagy induction since p62 is further decreased in the muscles of *Sting*^{-/-} mice compared with WT mice upon exercise (Fig. 3, F and G). Also, the protein level of LC3 is also further decreased in *Sting*^{-/-} mice compared with WT mice upon exercise (Fig. 3, F and G). These data indicate that autophagic flux is promoted in *Sting*^{-/-} mice, a phenotype similar to what we observed in *Drosophila*.

Moreover, we found that enhanced autophagic flux is accompanied by robust AMPK activation in *Sting*^{-/-} mice (Fig. 3, F and G). Among AMPK substrates, the phosphorylation levels of TSC2, Raptor, and TBC1D1 were significantly increased in the skeletal muscle of *Sting*^{-/-} mice without any effect on the phosphorylation of ACC (Fig. 4, A–F). We also found that STING deletion leads to markedly increased plasma membrane localization of GLUT4 in skeleton muscles after exercise labeled by Laminin2 (Bernet et al., 2014; Blanc et al., 2020; Liu et al., 2020;

Fig. 4, G and H), probably through AMPK-activated TBC1D1 phosphorylation for glucose uptake (Roach et al., 2007; Fig. 4, A–D). Enhanced activation of AMPK was also observed in STING KO MEFs upon starvation, and this enhanced AMPK activation was reversed in STING/STX17 double KO MEFs, indicating that STING regulates AMPK activity via STX17 mediated autophagy (Fig. 4 I).

STING deficiency elevates muscle glucose metabolism in mice

We further examined if energy metabolism is influenced in *Sting*^{-/-} mice. We observed that after exercise, blood glucose levels were greatly reduced in *Sting*^{-/-} mice compared with STING WT mice (Fig. 5 A) without affecting starting levels of glycogen in the liver and muscles (Fig. 5, B–E), TG levels in liver and gastrocnemius muscles (Fig. S1, A and B), circulating TG, FFA, lactate, glycerol, cholesterol, insulin levels (Fig. S1, C–H). Meanwhile, body weight, composition of the whole body, and daily food intake levels have no difference in STING KO and WT mice (Fig. S1, I–L). Also, there is no obvious difference in lipolysis in eWAT (Fig. S1, M and N), lipid droplet accumulation in the liver (Fig. S1 O), fatty acids oxidation (Fig. S1 P), and fatty acid uptake in muscles (Fig. S1, Q and R), consistent with unchanged ACC phosphorylation (Fig. 4, A–F). These data suggest that STING has a rather specific role in glucose metabolism upon acute exercise. Reduced blood glucose levels in STING KO mice are not caused by decreased glucose output in livers since we observed increased rather than decreased hepatic glucose output in STING KO mice than WT mice (Fig. 5, B–E), most likely due to a compensatory effect in response to blood glucose reduction. In addition, a significant increase in O₂ consumption, CO₂ production, and heat production was observed in the dark, in which mice are more active, in a Comprehensive Laboratory Animal Monitoring System (CLAMS; Fig. 5, F–I), supporting that there was an increased energy consumption in STING KO mice with the same locomotion in WT mice (Fig. 5, J and K). When carbohydrate is the predominant fuel source, the respiratory exchange ratio (RER; CO₂ production/O₂ uptake) value would approach 1.0; as fat provides most fuel, the RER value would be close to 0.7 (Simonson and DeFronzo, 1990). The increase of RER value (approaching to 1.0) in STING KO mice (Fig. 5 I)

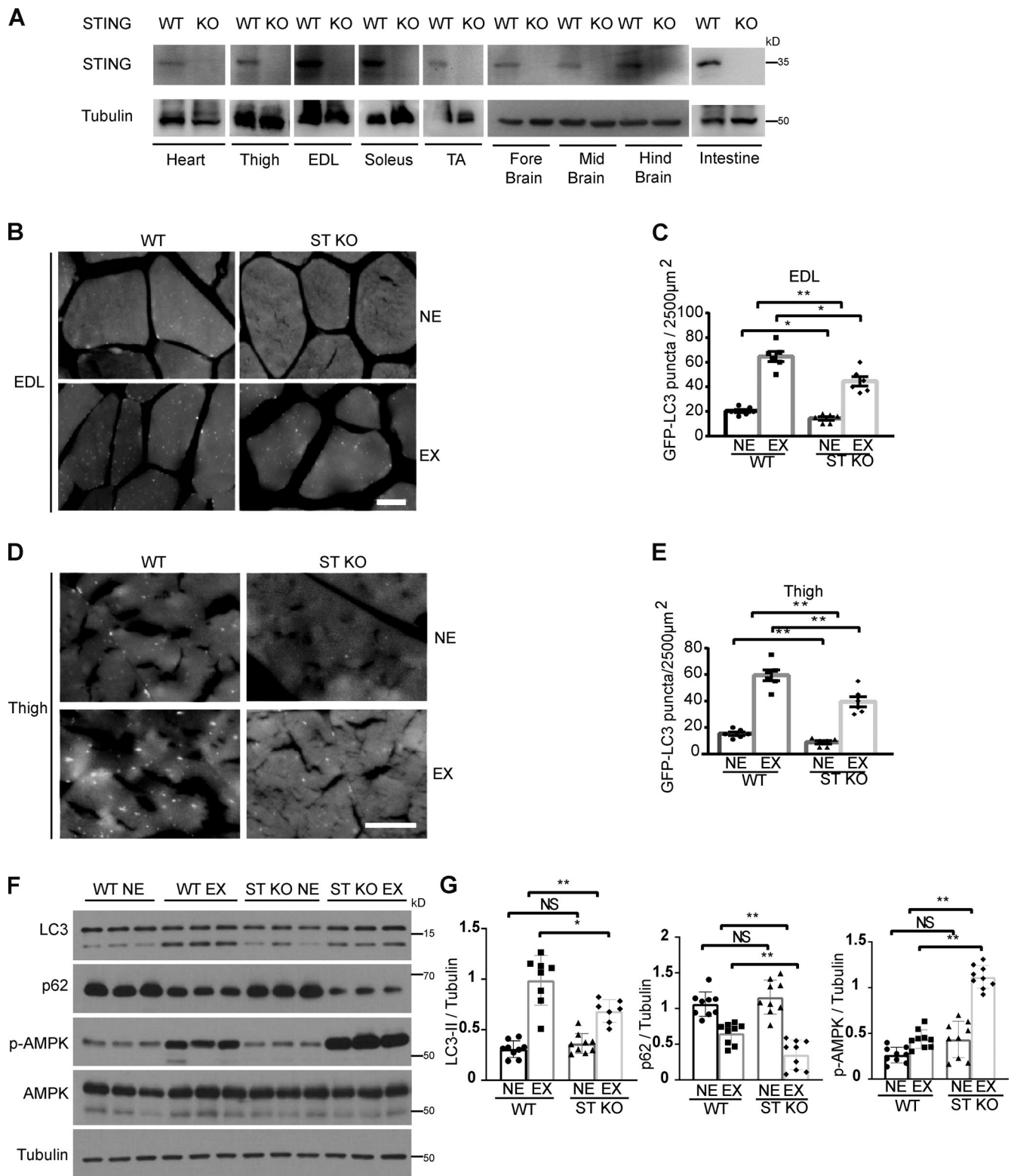


Figure 3. **STING** deficiency boosts exercise-induced autophagy in mice. **(A)** STING expression was examined in the indicated tissues of WT mice and STING KO mice. **(B–E)** Representative images of GFP-LC3 puncta in mouse skeletal muscle, including the extensor digitorum longus (EDL; B) and vastus lateralis (thigh; D) of GFP-LC3 WT and STING KO mice before and after exercise. NE, no exercise; EX, exercise. **(C and E)** Quantification of data (mean \pm SEM of 10 tissue sections) in B and D. *, $P \leq 0.05$; **, $P \leq 0.01$; ****, $P \leq 0.0001$. Scale bar, 20 μ m. **(F)** Immunoblot analysis of autophagic flux and AMPK phosphorylation (p-AMPK Thr172) in vastus lateralis muscle from three mice of the indicated genotypes before and after exercise. **(G)** Quantitative analysis of

autophagy and AMPK activities upon exercise. Immunoblot analysis of autophagic flux and AMPK phosphorylation (p-AMPK Thr172) in vastus lateralis muscle from mice of the indicated genotypes before and after exercise, *n* value as indicated below. Data are represented as mean \pm SEM. Unpaired two-tailed *t* test was used to compare different genotype for each condition. Two-way ANOVA for magnitude of changes between different conditions in mice of different genotypes. *, $P \leq 0.05$; **, $P \leq 0.01$; ***, $P \leq 0.0001$. Source data are available for this figure: SourceData F3.

acidification of GFP-RFP-LC3 by counting red only LC3 dots. The number of red-only LC3 dots was significantly increased in STING-KO cells compared with STING-complemented cells (Fig. 6, C and D). In addition, the suppression of autophagy by STING was also confirmed in HEK293T cells (that do not express endogenous STING or cGAS; Sui et al., 2017), in which ectopic expression of STING blocked the autophagic flux as shown by compromised degradation of LC3-II and p62 (Fig. 6 E). Moreover, we found STING did not affect the initiation of phagophore upon energy stress (Fig. S2, A–D). These data indicate that STING is important for autophagosome-lysosome fusion. We examined whether the role of STING in energy stress-induced autophagy is dependent on canonical autophagy machinery. Autophagic flux results show promoted degradation of LC3-II and p62 in STING deficient MEFs, whereas autophagy flux was blocked in STX17, ULK1/2, ATG14, ATG9A, and ATG5 depletion cells (Fig. 6, F and G). Furthermore, a series of canonical autophagy regulator expression levels were not changed in STING KO cells compared with WT cells (Fig. S2, E and F). These results suggest that STING negatively regulates autophagosome-lysosome fusion of energy stress-induced canonical autophagy in mammalian cells.

STING releases STX17 from ER in a stress-dependent manner

We found in *Drosophila* the increased degradation of Atg8a in both fed and starved conditions upon STING KO likely through the regulation of STX17 (Fig. 2, A–D). In MEF cells, the increased degradation of LC3 and p62 in Torin 1 treatment conditions upon STING KO can also be reversed by STX17 KO (Fig. 6 F). Both results suggest the promoted autophagy flux of energy stress-induced autophagy upon STING KO is very likely via regulation of the STX17.

STX17 contains two transmembrane domains and dynamically distributes to ER, ERGIC, Golgi, mitochondria, ER/Mito contact sites, and cytoplasm (Hamasaki et al., 2013; Itakura et al., 2012). In mammalian cells, upon autophagic stress, a portion of STX17 translocates to complete autophagosomes where it assembles SNAREpin with SNAP29 and lysosome resident VAMP8 to drive the fusion between autophagosomes and lysosomes (Itakura et al., 2012; Takats et al., 2013). To investigate the mechanism on how STING regulates energy stress-induced autophagy at the autophagosome-lysosome fusion step, we tested if ER-localized STING interacts with autophagic SNAREs, including STX17, SNAP29, and VAMP8. Endogenous STX17, but not SNAP29 or VAMP8, co-immunoprecipitated with STING (Fig. 7 A), suggesting that STING only interacts with STX17 but not the STX17-SNAP29-VAMP8 complex. This binding is conserved since dSTING also binds to *Drosophila* STX17 (dSYX17; Fig. 7 B). We then purified the cytosolic carboxyl terminus of STING from amino acid (aa) 139 to 379aa without its transmembrane domains inside ER lumen and performed the

reciprocal in vitro pull-down assays with STX17. The direct interaction between STING and STX17 was confirmed (Fig. 7, C and D). Although, the STING-STX17 interaction is rather specific, another autophagosome resident SNARE, Ykt6, which has been shown to participate in the autophagosome-lysosome fusion in the absence of STX17 (Matsui et al., 2018), failed to interact with STING (Fig. 7 E). We further investigated whether the interaction between STING and STX17 affects the assembly of autophagic SNAREpin STX17-SNAP29-VAMP8. Ectopic expression of STING disrupted the interaction between STX17 and SNAP29 or VAMP8 (Fig. 7 F). Further, the STX17-SNAP29-VAMP8 SNARE complex formation was increased upon STING depletion (Fig. 7 G), and the delivery of STX17 to autophagosome was also increased in STING KO cells (Fig. 7, H and I). STING depletion remarkably decreased STX17 distribution on ER structure compared with WT cells, with or without Torin 1 treatment (Fig. 7 J and Fig. S3 A). Upon autophagic stresses, including amino acid starvation, serum starvation, and Torin 1 treatment, the interaction between STING and STX17 is decreased as shown by reduced co-immunoprecipitation (Fig. 7 K). Consistently, the co-localization of STING with STX17 is dramatically decreased on autophagy induction (Fig. S3, B–D). These results indicate a pool of STX17 on ER was regulated by STING interaction upon autophagic stress stimulation. This pool of STX17 released by STING contributed to the increased amount of STX17 on autophagosome for autophagosome-lysosome fusion.

The phosphorylation of STX17 on S202 by TBK1 releases STX17 from STING and distributes STX17 to distinct structures

Considering STX17 has another function in autophagosome biogenesis, we then test whether STING interaction can also regulate this part of STX17 for autophagosome biogenesis. As reported, TBK1-phosphorylated STX17 at S202 translocates from Golgi to peripheral puncta during induction of autophagy to form mPAS (Kumar et al., 2019). We then investigated whether this pool of STX17 pS202 involved in autophagosome biogenesis is also regulated by the interaction with STING. To our surprise, The IP results showed STING interacted with the phosphorylation defective mutant STX17-S202A equally as STX17-WT, but the interaction was majorly abolished between STING and the constitutively active phosphorylation mutant STX17-S202D (Fig. 8 A). This highly suggested that the pool of STX17 retained by STING on ER is not phosphorylated by TBK1. Moreover, we examined the distribution of these two STX17 mutants. The results showed that STX17-S202D distributed on DFCP1⁺ mPAS structure, which is consistent with the previous report (Kumar et al., 2019; Fig. 8, B and C), but barely co-localized with both LC3 and LAMP2 (Fig. 8, D and E), while STX17-S202A preferred to distribute on LC3⁺-LAMP2⁺ mature autolysosomes (Fig. 8, D and E), but less distributed on DFCP1-labeled structure compared with the S202D mutant (Fig. 8, B and C). These results highly

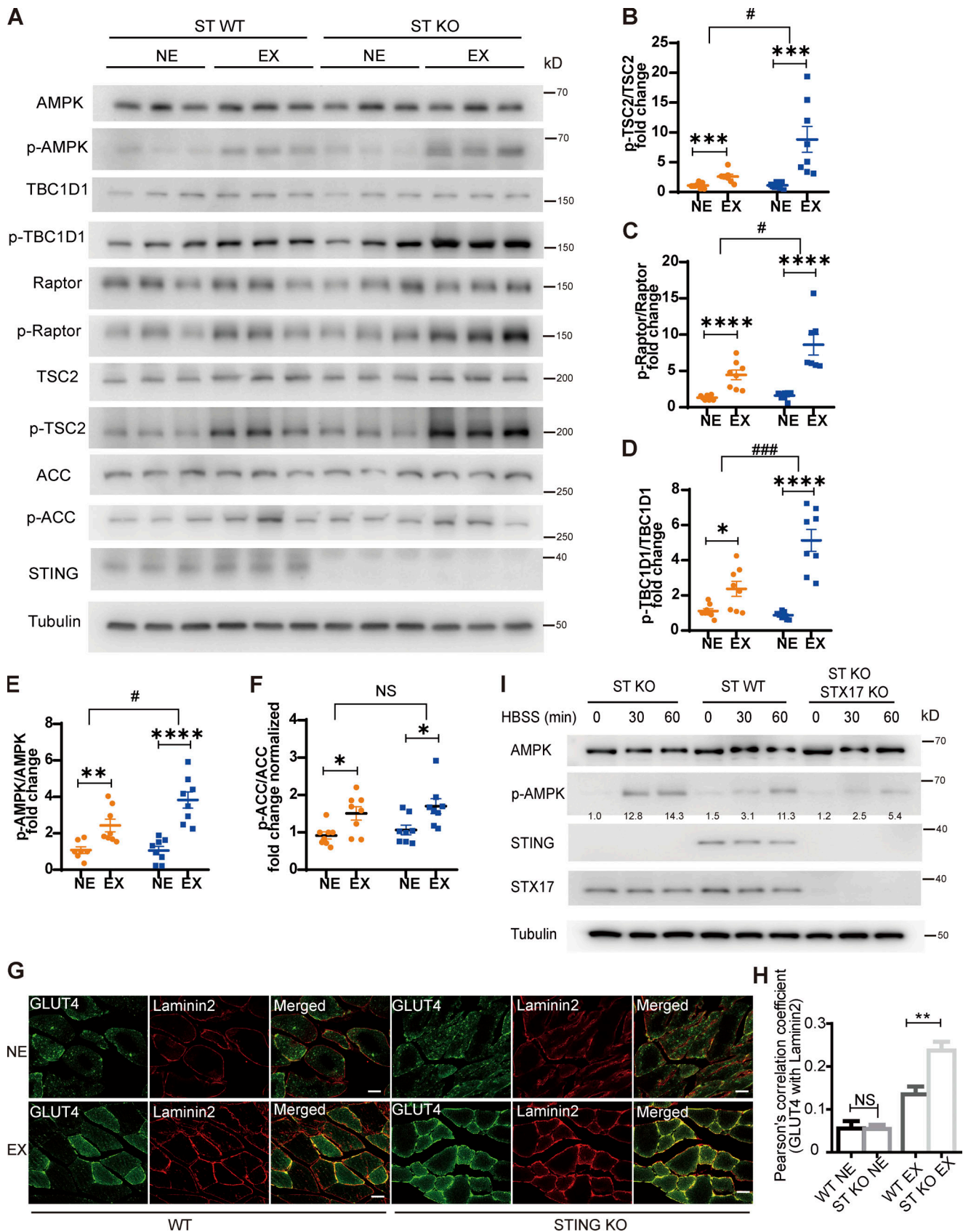


Figure 4. **STING depletion promotes AMPK and its substrates activation in mice muscle.** (A–F) Representative Western blots ($n = 3$; A) and quantification ($n = 6–8$) of the phosphorylation of AMPK (at Thr172; B) and its substrates TBC1D1 (at Ser237; C), Raptor (at Ser792; D), TSC2 (at Ser1387; E), and ACC (at Ser79; F) in gastrocnemius muscles from indicated genotypes before and after exercise. Data are represented as mean \pm SEM. ST, STING; NE, non-exercise; EX, exercise.

exercise; NS, not significant. *, $P \leq 0.05$; **, $P \leq 0.01$; ***, $P \leq 0.001$; ****, $P \leq 0.0001$. Unpaired two-tailed *t* test for comparison of two groups. Two-way ANOVA for comparison of magnitude of changes between different groups in mice of different genotypes. #, $P \leq 0.05$; ###, $P \leq 0.001$. **(G)** Increased GLUT4 translocation to plasma membrane in STING KO mice after exercise. Representative images of GLUT4 co-localization of Laminin2 in tibialis anterior muscles ($n = 4$). Scale bar, 20 μm . **(H)** Quantification of GLUT4 co-localization of laminin2 in tibialis anterior muscles ($n = 4$; G) are represented as mean \pm SEM. An area of 220.5 mm^2 per mouse was evaluated. NS, not significant; **, $P \leq 0.01$. Unpaired two-tailed *t* test for comparison of two groups. **(I)** AMPK activation analysis in STING WT, STING KO, and STING KO-STX17 KO cells. The STING WT, STING KO, and STING/STX17 DKO MEF cells were incubated in full medium or HBSS for the indicated time. AMPK phosphorylation (at Thr172) was detected by Western blot. Representative images were shown. The experiments were repeated three times and similar results were observed. Normalized fold change of p-AMPK/AMPK was listed. Source data are available for this figure: SourceData F4.

suggested the TBK1 phosphorylated pool of STX17 pS202 contributed to autophagy initiation but not autophagosome-lysosome fusion. All these observations nicely reconcile the different functions of STX17 in autophagy initiation and maturation. STING interacts with the non-phosphorylated form of STX17, which failed to interact with DFCP1, and this portion of STX17 dissociates from STING upon autophagic stress stimulation and translocates to mature autophagosome. On the other hand, TBK1 mediated STX17 pS202 abolished its binding with STING on ER, and this pool of STX17 pS202 contributes majorly to autophagosome biogenesis rather than autophagosome-lysosome fusion. Our hypothesis is that STING only affects the pool of STX17 on ER, which is not phosphorylated by TBK1, therefore mainly influencing autophagosome-lysosome fusion, but not autophagosome biogenesis. Indeed, this is consistent with our observation that the autophagosome formation upon Torin 1 treatment is not affected in STING KO MEFs compared with WT MEFs (Fig. S2, A–D), and also the protein levels of autophagy biogenesis related proteins are not altered between STING WT and KO cells (Fig. S2, E and F).

Effect of STING mutations on autophagy regulation

STING plays a central role in the cGAS-STING-TBK1-IFN pathway (Cai et al., 2014). Mutation of R232 to alanine disrupts cGAMP binding and therefore blocks ER exit of STING and prevents STING activation by DNA or cGAMP (Burdette et al., 2011; Dobbs et al., 2015; Zhang et al., 2013). Several gain-of-function mutations in STING were found in patients with an auto-inflammatory disease, namely STING-associated vasculopathy with the onset in infancy (SAVI; Liu et al., 2014) and more recently in patients with lupus-like syndromes (Jeremiah et al., 2014). Disease-associated STING mutants, N154S and V155M, lead to constitutive STING activation by driving STING trafficking from ER to ERGIC (bypassing the need for cGAMP; Dobbs et al., 2015; Jeremiah et al., 2014; Liu et al., 2014; Fig. S4 A). We next tested if the STING-STX17 interaction is affected by STING activation by its ligand cGAMP. We found that the interaction between STX17 and STING decreased upon cGAMP-mediated STING activation (Fig. 9 A); meanwhile STING homo-dimerization, which is essential for its activation, is not affected by STX17 overexpression (Fig. S4 B). STING WT and R232A (cGAMP binding defective mutant; Burdette et al., 2011) or S366A (phosphorylation and IFN signaling defective mutant; Tanaka and Chen, 2012) mutants failed to disrupt the STX17 binding and the STX17-SNAP29-VAMP8 complex assembly (Fig. 9 B), suggesting that the disruption of the STING-STX17 interaction requires cGAMP-mediated STING activation and ER exit. STING gain-of-function mutants N154S and V155M displayed enhanced binding to STX17 and a greater ability to

disrupt the STX17-SNAP29-VAMP8 complex (Fig. 9 C). All these STING mutants, capable of STING binding at ER/ERGIC, efficiently blocked autophagic flux (Fig. 9, D–F).

To identify a STING mutant that lost interaction with STX17, we first narrowed down the binding region of STING for STX17 to the cytosolic region aa134–160 (Fig. S4, C and D). Then random mutation was applied to the residues within this region of STING for STX17 binding. Through co-immunoprecipitation assays, we identified a STING C148A mutation, located at the connector helix (Shang et al., 2019), which reduces the STING-STX17 interaction by $\sim 50\%$ (Fig. 9 G). Consequently, STING-KO MEFs stably expressing STING C148A mutant displayed a compromised inhibitory effect in autophagic flux analysis (Fig. 9 H). In contrast to STING binding defective C148A mutant, STING WT, R232A, S366A, N154S, and V155M mutants all displayed inhibitory activity as shown by the accumulation of LC3 puncta, failure of STX17 to localize to autophagosomes, and defective autophagosome acidification (Fig. 9, I–K, Fig. S4 E, Fig. S5, and Fig. S6).

STX17 and STING translocate to different types of autophagic vacuoles upon DNA stimulation

Upon HT-DNA activation, we found that STX17 translocates to LC3-labeled mature autophagosomes, but not to STING and LC3 double-positive vesicles (Fig. 10, A and B), suggesting that STX17 dissociates from STING and uncouples from STING-mediated non-canonical autophagy, which is consistent with the reduced interaction between STX17 and STING upon DNA activation (Fig. 9 A). Lastly, since STING likely activates both DNA-mediated non-canonical autophagy and STX17-mediated energy stress-induced autophagy, we tested if energy stress-induced autophagy activation affects innate immunity response. Activation of energy stress-induced autophagy by mTORC1 inhibitor Torin 1 significantly compromised the IFN expression upon DNA treatment (Fig. 10, C and D). In STX17-KO MEFs, neither STING degradation (Fig. 10 E) nor STING translocation (Fig. 10 F) was affected compared with the WT MEFs (Fig. 10, E and F), further supporting that the STING-mediated PAMPs-induced non-canonical autophagic pathway is distinct from the STING-STX17 regulated canonical autophagic pathway. In summary, we conclude that STING inhibits autophagosomal fusion with lysosomes through its interaction with STX17 at ER/ERGIC, and this inhibition could be released by STING activation by cGAMP and trafficking away from ER/ERGIC or STING depletion.

Discussion

This study demonstrates the crucial role of STING in glucose metabolism through its negative regulation in energy stress-

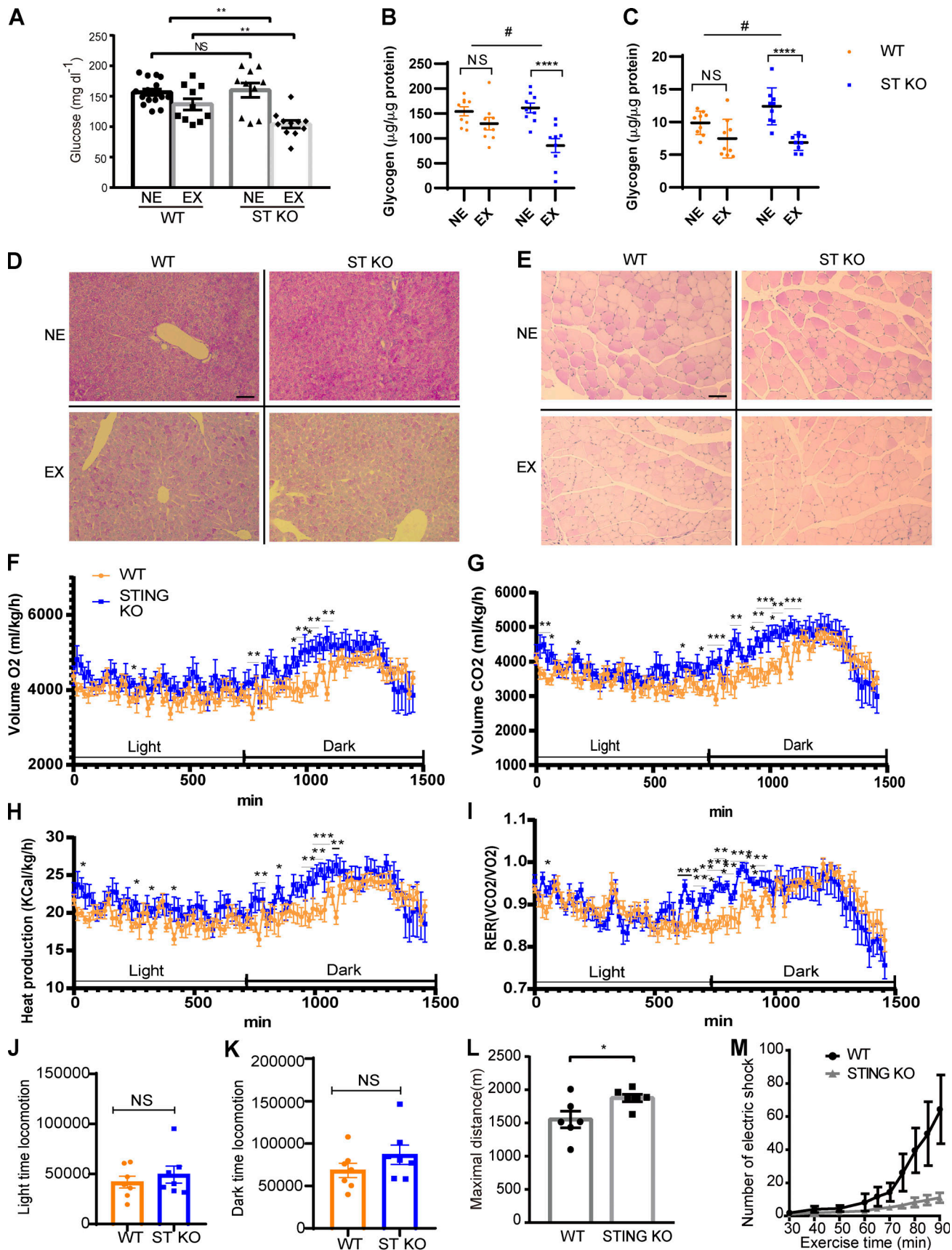


Figure 5. **STING KO mice exhibited increased glucose consumption and metabolic changes.** (A) Plasma glucose levels in mice with indicated genotypes before and after exercise. Data represent mean ± SEM of 10–15 mice per group. (B and C) Glycogen content in mice liver (B) and TA muscle (C; n = 9) with

indicated genotypes before and after exercise. **(D and E)** Representative images of PAS staining in mice liver (D) and thigh muscle (E) with indicated genotypes before and after exercise. Scale bars, 100 μ m. **(F–I)** Oxygen consumption (VO_2 ; F), carbon dioxide release (VCO_2 ; G), heat production (H), respiratory exchange ratio (I) of STING WT or STING KO mice ($n = 7$). **(J and K)** Locomotion activity of WT and STING KO mice. The light (J) or dark (K) time locomotion were measured in 8–12 wk old WT and STING KO mice using CLAMS ($n = 7$). Data were collected every 16 min. Data are represented as mean \pm SEM. ST, STING; NE, non-exercise; EX, exercise. **(L)** Maximal treadmill running distance for mice with indicated genotypes. Data represent mean \pm SEM of five mice per group. **(M)** Electrical shock counts in STING WT and KO mice. Electrical shock number of separated treadmill lanes were collected and shown in 8–12 wk old WT and STING KO male mice ($n = 6$) during a 90 min exercise program. Data are represented as mean \pm SEM. NS, not significant; *, $P \leq 0.05$; **, $P \leq 0.01$; ***, $P \leq 0.001$; ****, $P \leq 0.0001$; #, $P \leq 0.05$. Unpaired two-tailed *t* test for comparison of two groups. Two-way ANOVA for comparison of magnitude of changes between different groups in mice of different genotypes.

induced autophagy. The connection between autophagy and the cGAS-STING pathway has been intensively investigated with a focus on pathogens, DNA, or cyclic dinucleotides-induced autophagy through a non-canonical pathway (Gui et al., 2019; Liang et al., 2014; Liu et al., 2019; Watson et al., 2012). Here, we found that STING also plays a crucial role in energy stress-induced autophagy, especially in autophagosome-lysosome fusion through its interaction with the autophagic SNARE STX17. In the unstressed conditions, STING physically interacts with STX17 and sequesters it at ER. This interaction is disrupted by STING activation (DNA treatment etc) or autophagy stimuli (energy stress, etc.), which leads to STX17 translocation to autophagosomes, assembly of autophagic SNARE complex, and promotion of autophagosomal fusion with lysosomes. STING-regulated energy stress-induced autophagy has at least two effects, to facilitate elimination of DNA and microbes in immune cells and to boost energy metabolism in non-immune cells.

STX17 is also important for autophagosome biogenesis. How the functions of STX17 in autophagy initiation and autophagosome-lysosome fusion is differentiated is an interesting question. We propose that STX17 phosphorylation by TBK1, as described by Kumar et al. (2019), likely separates these two functions. TBK1-phosphorylated STX17 translocates from Golgi to mPAS, which is not controlled by STING, while the portion of STX17 that is not phosphorylated by TBK1 interacts with STING at ER/ERGIC, and this interaction is disrupted by autophagic stress likely through TBK1-independent regulatory events, which leads to translocation of this portion of STX17 from ER/ERGIC to complete autophagosomes. These observations nicely reconcile the different functions of STX17 in autophagy initiation and maturation.

STING-regulated energy stress-induced autophagy is different from previously reported STING-mediated non-canonical autophagy in several aspects: (1) different membrane trafficking pathways are utilized. Triggered by PAMPs, STING translocates to single bilayer membrane vesicles (Saitoh et al., 2009) positive for LC3, but these STING-LC3 positive vesicles are negative for STX17; (2) PAMPs-triggered STING-mediated autophagy is independent of BECN1, ULK1, and Atg9a (Gui et al., 2019; Liu et al., 2019). STX17 neither localizes to STING-positive vesicles nor is it required for STING trafficking and degradation; (3) PAMPs-induced non-canonical autophagy is compromised when STING is absent; while canonical autophagy is further activated in the absence of STING given that more STX17 is released from ER; (4) PAMPs-induced STING-dependent autophagy activation is limited to immune cells, but STING-regulated

canonical autophagy functions broadly in both immune and non-immune cells.

STING is a crucial regulator in the cancer-immunity cycle, and activation of STING represents a promising strategy for cancer therapy. Our study suggests, in addition to immunity regulation, activation of STING also promotes energy stress-induced autophagy by releasing STX17 from ER. How autophagy activation contributes to STING mediated signaling remained to be investigated. At least, our study indicates that STING might play an unexpected broader role in energy metabolism due to its regulation of energy stress-induced autophagy. Autophagy has been implicated in a broad spectrum of human diseases, and STING also expresses and functions in non-immune tissues, suggesting that the regulatory effect of STING on autophagy might contribute to the pathogenesis of autophagy-related diseases and immune functions.

Materials and methods

Antibodies and reagents

Antibodies used in this study included anti-STING (13647; Cell Signaling Technology), anti-Flag M2 (F3165; Sigma-Aldrich), anti-HA (H3663; Sigma-Aldrich), anti-EGFP (GL-8; Clontech), anti-LC3 (7543; Sigma-Aldrich), anti-p62 (PM045; MBL), anti-STX17 (HPA001204; Sigma-Aldrich), anti-SNAP29 antibody (111303, SYSY, or sc-135564; Santa Cruz Biotechnology), anti-LAMP1 (L1418; Sigma-Aldrich), anti-LAMP2 (sc-18822; Santa Cruz or LO668; Sigma-Aldrich), anti-Myc (9E10, DSHB), anti-WIP1 (ab105459; Abcam), anti-FIP200 (17250; ProteinTech), anti-ATG16L (PM040; MBL), anti- α -Tubulin (E7; DSHB), anti-VAMP8 (ab76021; Abcam), anti-GABARAP (ab109364; Abcam), anti-AMPK (2532; Cell Signaling Technology), anti-p-AMPK T172 (2535; Cell Signaling Technology), anti-TBC1D1 (66433; Cell Signaling Technology), anti-p-TBC1D1 Ser237 (07-2268; Sigma-Aldrich), anti-Raptor (2280; Cell Signaling Technology), anti-p-Raptor Ser792 (2083; Cell Signaling Technology), anti-TSC2 (4308; Cell Signaling Technology), anti-p-TSC2 Ser1387 (5584; Cell Signaling Technology), anti-ACC (3662; Cell Signaling Technology), anti-p-ACC Ser79 (3661; Cell Signaling Technology), anti-Glut4 (GT-41-A; Alpha diagnostic international), anti-Laminin2 (LO663; Sigma-Aldrich), anti-CD36 (80080; Abcam), anti-Dystrophin (15277; Abcam), and LysoTracker (ENZ-51005; Enzo).

Cell culture and cell transfection

HEK293T, MEF, and U₂OS cells were cultured in DMEM (Gibco) supplemented with 10% FBS (HyClone) and 1%

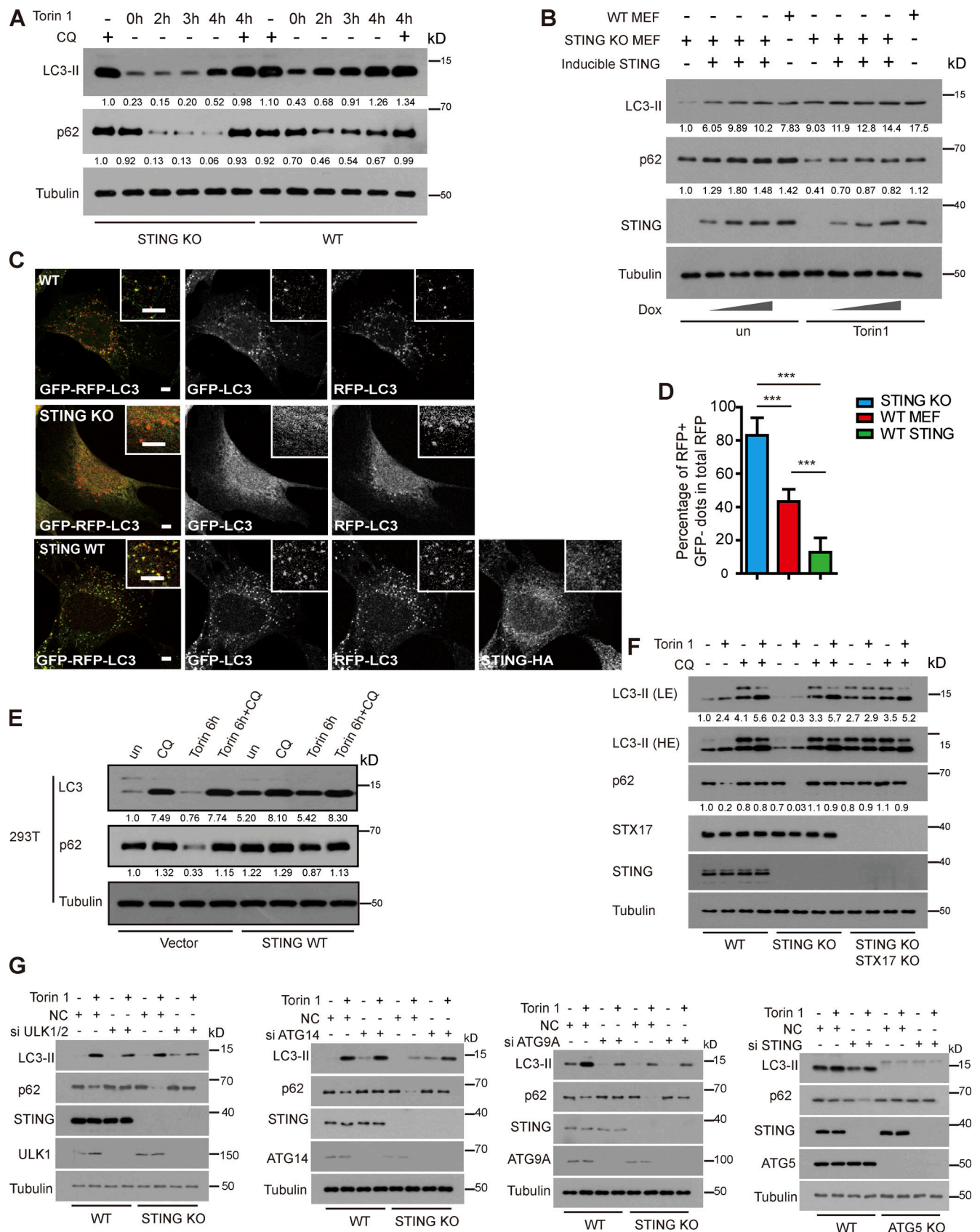


Figure 6. **STING** inhibits autophagosome-lysosome fusion. **(A)** Autophagic flux is accelerated in STING-KO MEFs compared with WT MEFs. WT MEFs and STING-KO MEFs were treated with Torin 1 with or without CQ for the indicated time and then immunoblotting was performed with indicated antibodies. Normalized fold change of LC3II/Tubulin or p62/Tubulin was listed. **(B)** Inducible expression of STING at endogenous level inhibits autophagic flux in MEFs.

Inducible stable cell line expressing STING was treated with different doses of doxycycline (0, 100, 200 ng/ml) for 24 h to induce STING expression. After 24 h, WT MEFs, STING-KO MEFs, and STING-KO MEFs reconstituted with inducible STING were treated with or without Torin 1 for 3 h. Cells were lysed and immunoblotting was performed with indicated antibodies. Normalized fold change of LC3II/Tubulin or p62/Tubulin was listed. **(C)** Fusion between autophagosomes and lysosomes is promoted in STING-KO MEFs. WT MEFs, STING-KO MEFs, and STING-KO MEFs reconstituted with STING-HA were treated with Torin 1 for 3 h before fluorescence of GFP-RFP-LC3 was imaged. Scale bar, 5 μ m. **(D)** Quantification of the results in C. Percentage of RFP + GFP-dots in total RFP dots. Data are mean \pm SD for 100 cells. ***, $P \leq 0.001$. **(E)** Expression of STING-HA inhibits the autophagic flux in HEK293T cells. HEK293T cells were transfected with empty vector, WT STING-HA. 24 h after transfection, cells were treated with Torin 1 combined with or without CQ for indicated time. Immunoblotting was performed with indicated antibodies. Normalized fold change of LC3II/Tubulin or p62/Tubulin was listed. **(F and G)** STING regulated autophagosome-lysosome fusion is STX17 (F), ULK1, ATG9, ATG14, and ATG5 (G) dependent. Immunoblot analysis of LC3-II conversion and p62 degradation in MEFs and STING KO MEFs transfected with the indicated siRNAs. Immunoblot analysis of LC3-II conversion and p62 degradation in MEFs and ATG5 KO MEFs transfected with the siRNAs against STING. NC, Non-target control. Normalized fold change of LC3II/Tubulin or p62/Tubulin was listed. Source data are available for this figure: SourceData F6.

penicillin-streptomycin solution (Gibco). Cell transfection was performed using Lipofectamine 3000 (Invitrogen) or PEI (Polysciences) according to protocols provided by the manufacturers. STING WT, STING KO, and STING KO expressing STING-HA MEF cells were from Nan Yan Lab as described previously (Gonugunta et al., 2017).

Plasmids

The STX17, SNAP29, and Vamp8 expression plasmids were mentioned in a previous study (Diao et al., 2015). STING-HA constructs were from Nan Yan Lab, and the mutations of STING-HA or Myc-, Flag-STX17 were prepared by Q5 polymerase (M0491; NEB) and then digested by DpnI (RO176; NEB) endonuclease. The sgRNA oligo used in CRISPR/Cas9 KO of STX17 in STING WT or STING KO MEF cells is 5'-AGGAAAAGGTGAAGT TACGC-3'. For knockdown of ULK1, the siRNA oligos are: 1, 5'-GGGUAGUAAUGACACCACCUCGGAA-3'; and 2, 5'-GAACCTTGC CAAGTCCCAAACACTG-3'; for knockdown of ULK2, the siRNA oligos are: 1, 5'-GTTAAAAATCTGAATGAAAGATACA-3'; and 2, 5'-AGGATAGAATGGACTTTGAAGCATT-3'; for knockdown of ATG14, the siRNA oligos are: 1, 5'-GCAAGAUGAGGAUUGAACAA-3'; and 2, 5'-GGGTCTGTGATGACCACAA-3'; for knockdown of ATG9A, the siRNA oligos are: 1, 5'-GUACAUGAAUUGCUUCUUG-3'; and 2, 5'-CCCAGCTCTTCCAGTACAA-3'.

Immunofluorescence staining

Cells were grown on coverslips and transfected according to protocols provided by manufacturers with noted plasmids. After 24 h, cells were fixed using ice-cold 4% PFA for 10 min. Cells were then washed three times with PBS and blocked with blocking buffer (4% BSA + 0.1% Saponin in PBS) at 25°C for 30 min. Cells were incubated with primary antibodies at 4°C overnight, washed three times with PBS buffer, and then incubated with appropriate secondary antibodies for 1 h at 25°C. Slides were examined under a laser scanning confocal microscope (Zeiss LSM 880) using 63 \times (NA 1.4) or 40 \times (NA 1.3) lenses at RT. For immunofluorescence staining of skeletal muscles sections, mice were perfused with 4% PFA. Skeletal muscles were dissected and fixed in 4% PFA overnight, and then incubated in 15% sucrose in PBS for 4 h or overnight followed by an incubation of 30% sucrose in PBS overnight before the frozen sections were prepared. After freezing the sections, the skeletal muscles sections were stained with primary antibodies and the appropriate secondary antibodies. Sections were mounted and

imaged using a fluorescent microscope (Zeiss Axioplan2) under a 63 \times (NA 1.4) lens at RT. For GFP-LC3 imaging, the sections were directly mounted, and images were taken using a fluorescent microscope (Zeiss Axioplan2) under a 63 \times (NA 1.4) lens at RT.

Immunoprecipitation assays

Cells were lysed using buffer (20 mM Tris-HCl, pH 7.5, 150 mM NaCl, 0.5% Igepal CA-360, 1 mM NaF, 1 mM Na₃VO₄, 1 mM EDTA, and a protease inhibitor mixture) on ice. Whole-cell lysates were collected after 12,000 *g* centrifugation. The lysate was then incubated with anti-Flag (Sigma-Aldrich), anti-HA (Sigma-Aldrich), or anti-Myc Affinity Gel (Bimake) for 16 h at 4°C. Beads were washed three times with lysis buffer and then were dissolved in 2 \times loading buffer for SDS-PAGE. Immunoblotting was performed following standard procedures.

In vitro binding assay

His-STING (139aa-379aa) was expressed and purified as previously described (Tanaka and Chen, 2012). Full-length GST, GST-STX17, FLAG-STX17, FLAG-VAMP8, and FLAG-SNAP29 were expressed individually with amino-terminal TEV protease cleavable GST tag in *Escherichia coli* strain BL21(DE3) at 25°C. All proteins were purified according to previously described protocols (Diao et al., 2015). In GST pull-down assays, GST and GST-STX17 were applied to the GST resin. Then 1 μ g SNAP29 and 1 μ g STING-His (139aa-379aa) were added respectively and incubated overnight. Proteins were eluted by reduced glutathione and dissolved in sample buffer for SDS-PAGE and immunoblotting. In His pull-down assay, 1 μ g FLAG-tagged proteins and 1 μ g His-tagged STING (139aa-379aa) were incubated overnight with Nickel NTA resin (Qiagen) and then dissolved in sample buffer for SDS-PAGE and immunoblotting.

Autophagy assays

Autophagy activity was assessed by fluorescence microscopy, measuring GFP-LC3-positive puncta in cells and tissue sections from mice with transgenic expression of GFP-LC3 (Mizushima et al., 2004) or using the RFP-GFP-LC3 assay, or by immunoblot analysis of LC3-II conversion and p62 levels.

Drosophila experiments

Flies were maintained using standard conditions. The Bloomington Stock Center provided Da-Gal4, Arm-Gal4 driver lines, and the STING RNAi line (CG1667, BS31565). UAS-GFP LAMP

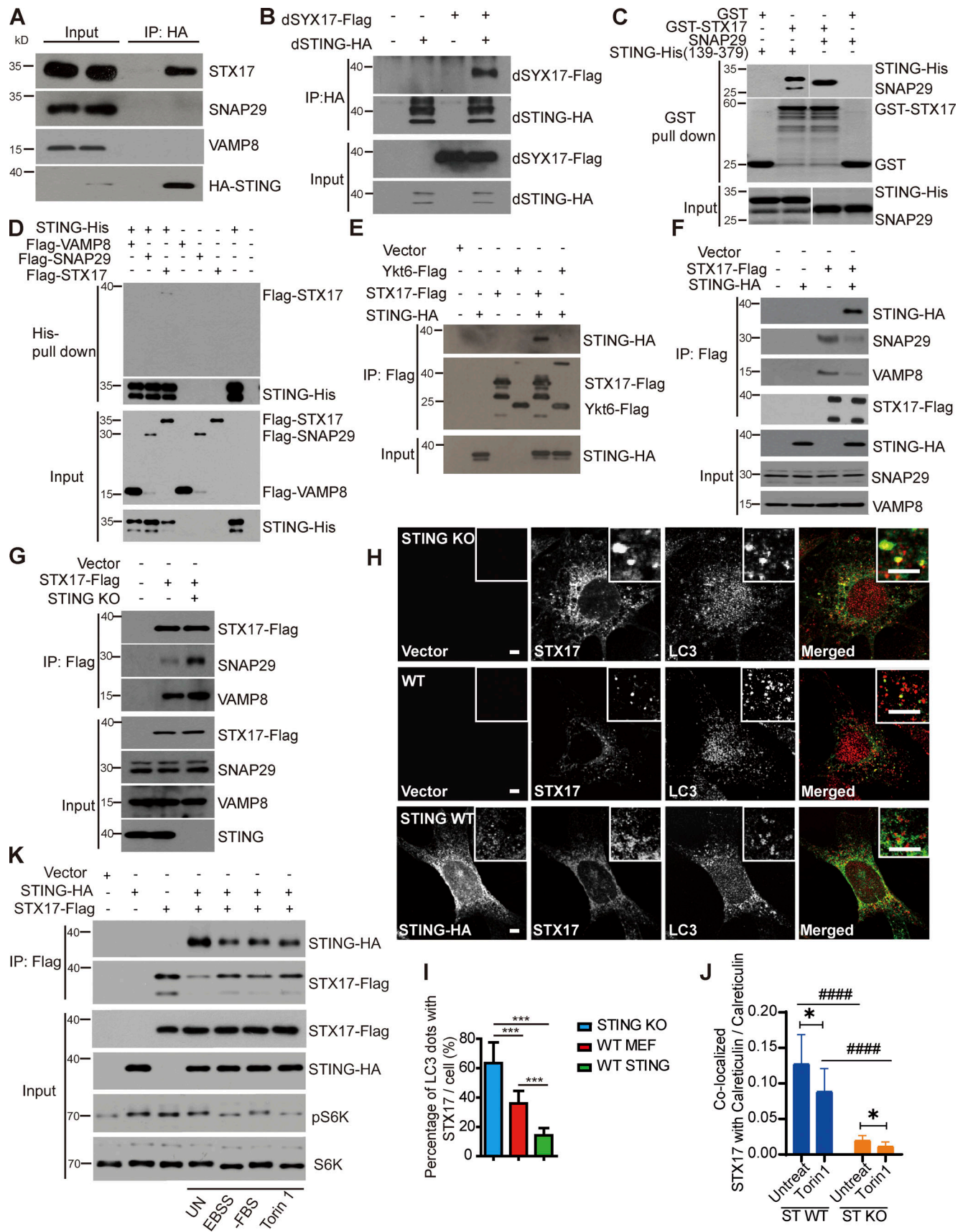


Figure 7. **STING sequesters STX17 at ER in a stress dependent manner.** (A) STING-HA interacts with endogenous STX17, but not SNAP29 and VAMP8. HEK293T cells were transfected with empty vector or STING-HA. 24 h after transfection, cells were lysed and immunoprecipitated with anti-HA antibody.

(B) dSTING-HA interacts with dSYX17. HEK293T cells were transfected with empty vector, dSTING-HA, dSTX17-Flag with or without dSTING-HA. 24 h after transfection, cells were lysed and immunoprecipitated with anti-HA antibody. Immunoblotting was performed with indicated antibodies. **(C)** Direct binding of GST-STX17 to STING-His (139aa–379aa) and SNAP29 in vitro. Glutathione sepharose beads bound with GST or GST-STX17 were incubated with purified SNAP29 or STING-His (139aa–379aa) for 16 h and then eluted for immunoblotting. **(D)** Direct binding of STING-His (139aa–379aa) to Flag-STX17, but not Flag-SNAP29 or Flag-VAMP8 in vitro. Nickel NTA resin bound with STING-His (139aa–379aa) was incubated with Flag-STX17, or Flag-SNAP29, or Flag-VAMP8 for 16 h, and then eluted for immunoblotting. **(E)** STING-HA interacts with STX17-Flag, but not with Ykt6-Flag. HEK293T cells were transfected with empty vector, STX17-Flag, Ykt6-Flag with or without STING-HA. 24 h after transfection, cells were lysed and immunoprecipitated with anti-Flag antibody. Immunoblotting was performed with indicated antibodies. **(F)** Overexpression of STING-HA disrupts the interaction of STX17-Flag with SNAP29 and VAMP8. HEK293T cells were transfected with empty vector, STX17-Flag with or without STING-HA. 24 h after transfection, cells were lysed and immunoprecipitated with anti-Flag antibody. Immunoblotting was performed with indicated antibodies. **(G)** STING depletion increases STX17–SNAP29–VAMP8 SNARE complex formation. WT and STING-KO MEFs expressing STX17-Flag were lysed and immunoprecipitated with anti-Flag antibody and immunoblotting was performed with indicated antibodies. **(H)** STING blocks the translocation of STX17 to autophagosomes. WT MEFs, STING-KO MEFs, and STING reconstituted STING-KO MEFs with stable expression of STX17-Flag were treated with Torin 1 for 3 h and stained with antibodies against Flag, HA, and LC3. Scale bar for both large and inset images, 5 μ m. **(I)** Quantification of the results in H. Percentage of LC3 dots with STX17. Data are mean \pm SD for 100 cells. ***, $P \leq 0.001$. Unpaired two-tailed t test for comparison of two groups. **(J)** The statistics result of Fig. S3 B indicates that STX17 co-localized with Calreticulin marked ER in STING WT or STING KO MEF cells expressing Flag-STX17 after treatment with Torin 1 for 3 h or no treatment, then cells were conducted immunofluorescence and imaging. Over 30 cells were analyzed. Data are represented as mean \pm SD. *, $P \leq 0.05$; ****, $P \leq 0.001$. Unpaired two-tailed t test for comparison of two groups. **(K)** Interaction between STING-HA and STX17-Flag is decreased upon EBSS starvation, serum starvation, and Torin 1 treatment. HEK293T cells were transfected with empty vector, STING-HA with or without STX17-Flag. 24 h after transfection, cells were starved with EBSS, FBS deprived medium or treated with Torin 1 followed by immunoprecipitation with anti-Flag antibody. Source data are available for this figure: SourceData F7.

transgenic flies were generated as described (Pulipparacharuvil et al., 2005). A *dSting* null allele was generated by replacing the promoter, start codon, and the first 66 amino acids with a 3xP3-DsRed cassette using a standard CRISPR/Cas9 approach (Gratz et al., 2015). gRNAs expressed from the pU6-Bbs1 plasmid targeted the following sequences flanking the deleted region in the *dSting* gene: 5'-CGAGATCTCCAAATCGATC-3' and 5'-TCGTGCAATATGGGAGCAA-3'.

Fly stocks were maintained under RT using standard conditions. Bloomington *Drosophila* Stock Center provided w^{1118} , Da-Gal4, Arm-Gal4 driver lines, and the *Sting* RNAi line (CG1667, BS31565). UAS-GFP LAMP transgenic flies have been described (Pulipparacharuvil et al., 2005). UAS-Myc-dSyx17 and UAS-dSting-3xTy1 transgenes were generated by standard cloning in a pAttB-UAS vector for site-specific insertion at the AttP sites VK00014 at 43A1 or VK00027 at 89E11, respectively. A *dSting* null allele was generated by replacing promoter, start codon, and the first 66 amino acids with a 3xP3-DsRed cassette using a standard CRISPR/Cas9 approach (Gratz et al., 2015). gRNAs expressed from the pU6-Bbs1 plasmid targeted the following sequences flanking the deleted region in the *dSting* gene: 5'-CGAGATCTCCAAATCGATC-3' and 5'-TCGTGCAATATGGGAGCAA-3'. The *Syx17^[LL]* mutant was a kind gift from Dr. Gabor Juhász (Takats et al., 2013). Experiments with UAS-RNAi transgenes were performed at 28°C to maximize knockdown efficiency and all other crosses were performed at 25°C.

Quantitative real time PCR

Quantitative RT-PCR was used to measure transcript levels of *dSting* in Da-Gal4 and Arm-Gal4-driven *Sting* knockdown larvae. Briefly, RNA was isolated using TRIZOL (Ambion) according to the manufacturer's instructions. 2 μ g RNA was reverse transcribed using High-Capacity cDNA Reverse Transcription kit (Applied Biosystems) using random hexamer primers. Quantitative PCR was performed using the Fast SYBR Green Master Mix in a real-time PCR system (Fast 7500; Applied Biosystems). Each data point was repeated three times with independent samples and normalized with ribosomal rp49 gene as an

internal control. *dSting* primers were: left, 5'-ACGTACTCTAAC TTGTGGGT-3' and right, 5'-CAATTCGCCAACATCCACCA-3', and rp49 primers were: left, 5'-ATCGGTTACGGATCGAACAA-3' and right, 5'-GACAATCTCCTTGGCTTCT-3'.

Histology

Whole-mount larval fat bodies were prepared for immunofluorescence staining as previously described (Nandi et al., 2017). Briefly, dissected fed and starved samples were fixed in periodate-lysine-PFA, washed in PBS, permeabilized with 0.3% saponin in PBS (PBSS), blocked with 5% goat serum in PBSS, stained with rabbit anti-GABARAP (1:200; Abcam, ab109364; detects endogenous ATG8a), and labeled with Alexa Fluor 488 (1:500; Molecular Probes) secondary antibody and mounted in Vectashield containing DAPI (Vector Laboratories). Fluorescence images were captured with 63 \times (NA 1.4) or 40 \times (NA 1.3) or 20 \times (NA 0.75) lenses on an inverted confocal microscope (LSM710 or LSM510 Meta; Zeiss). Confocal Z-stacks of tissues were collected at a 1- μ m step size and processed using ImageJ and Adobe Photoshop. For autophagic flux experiments, 72-h old larvae were transferred to a fresh medium containing 3 mg/ml CQ (Sigma-Aldrich) for a 24-h treatment as described before (Low et al., 2013). Over-expression and RNAi knock-down clones were generated by heat shocking 3-d old larvae carrying *hsFLP*, *actin>CD2>Gal4*, UAS-GFP, and the indicated UAS-transgenes at 38°C for 1 h the day prior to dissection. LysoTracker (GFP-Certified Lyso-ID red lysosomal detection kit; Enzo Life Sciences) staining of size-matched 92–94 h fat bodies from fed and starved larvae was performed as previously described (Nandi et al., 2017). Briefly, larvae were dissected in Schneider's Insect Media (Gibco), inverted to expose fat bodies, and incubated in 100 μ M LysoTracker Red DND-99 for 1 min. Inverted carcasses were then washed in 1 \times PBS and fat bodies were mounted in a droplet of Vectashield (Vector Laboratories). Samples were imaged immediately on an inverted confocal microscope (LSM 710 using 63 \times , NA 1.4 Plan Apochromat lens). Z projections of three optical sections of fat body tissue, each 1 μ m apart, were used to quantify LysoTracker and Atg8a puncta in fat

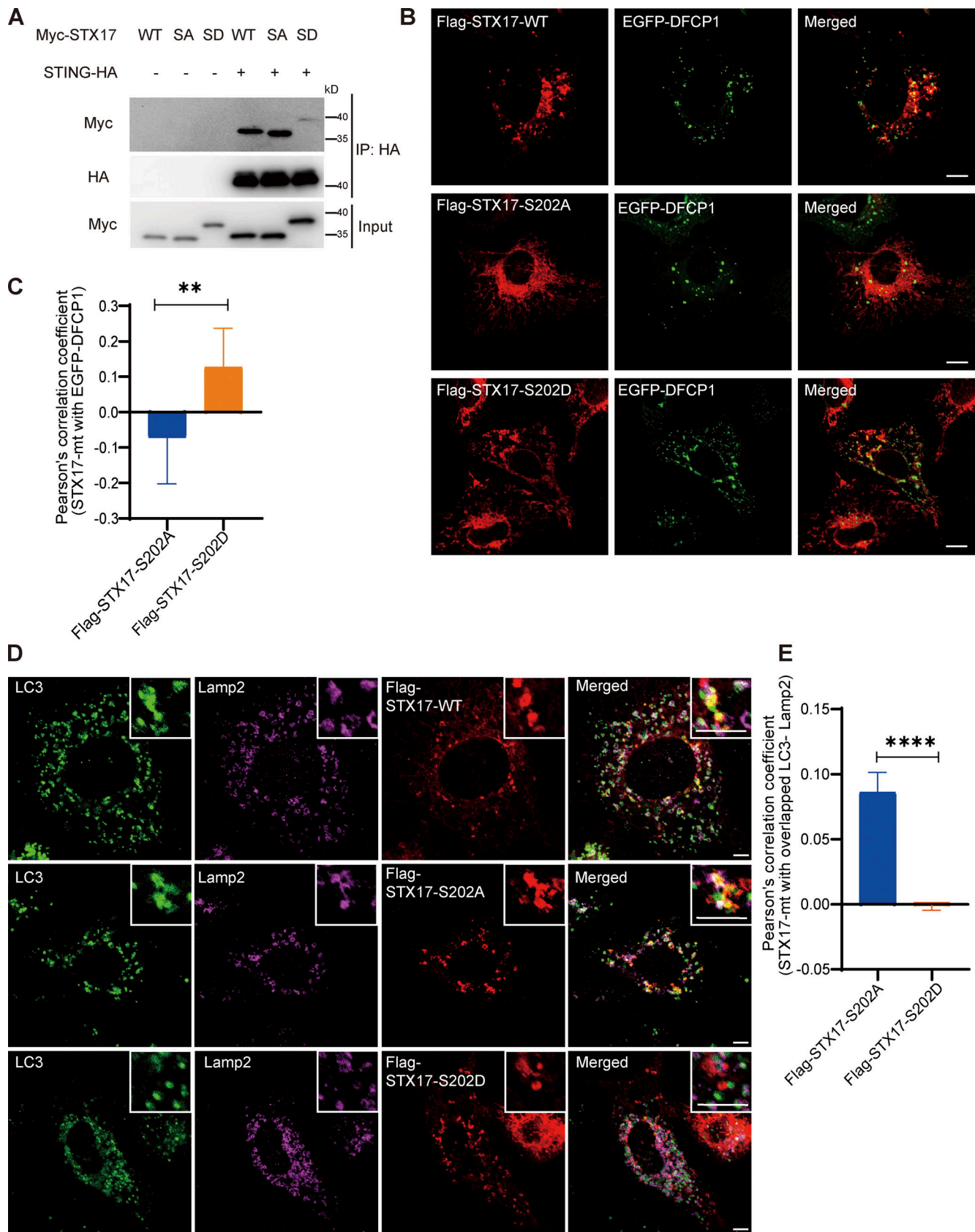


Figure 8. **The phosphorylation of STX17 on S202 by TBK1 releases STX17 from STING and distributes STX17 to distinct structures.** (A) STING interaction with STX17 was inhibited TBK1 phosphorylation on STX17 S202. HEK293T cells were transfected with empty vector or STING-HA, combined with Flag-STX17-WT or Flag-STX17-S202A (SA) or Flag-STX17-S202D (SD) as indicated. 24 h after transfection, cells were lysed and immunoprecipitated with anti-

HA agarose resin. **(B)** Flag-STX17-S202D co-localized with phagophore structure to a larger extent. U2OS cells were transfected with Flag-STX17 or Flag-STX17-S202A or Flag-STX17-S202D, combined with EGFP-DFCP1. After treated with Torin 1 for 3 h, cells were fixed and stained by indicated antibody and imaged by confocal microscopy. Representative images were shown. Scale bar, 10 μ m. **(C)** Statistics result of B, representing co-localization between Flag-STX17-S202A or Flag-STX17-S202D with EGFP-DFCP1 in U2OS cells co-expressing plasmids as indicated and treated with Torin 1 for 3 h. At least 30 cells were analyzed. Data were mean \pm SD. **, $P \leq 0.01$. Unpaired two-tailed *t* test for comparison of two groups. **(D)** Flag-STX17-S202A better co-localized with complete autophagosome. U2OS cells were transfected with Flag-STX17 or Flag-STX17-S202A or Flag-STX17-S202D. After being treated with Torin 1 for 3 h, cells were fixed and stained by indicated antibody and imaged by confocal microscopy. Representative images were shown. Scale bars for both large and inset images, 10 μ m. **(E)** Statistics result of D, representing co-localization between Flag-STX17-WT or Flag-STX17-S202A or Flag-STX17-S202D with overlapped LC3-Lamp2 area in U2OS cells expressing plasmids as indicated and treated with Torin 1 for 3 h. At least 30 cells were analyzed. Data were mean \pm SD. ****, $P \leq 0.0001$. Unpaired two-tailed *T* test for comparison of two groups. Source data are available for this figure: SourceData F8.

bodies using Imaris software (Bitplane) or ImageJ. The number of punctate was quantified per fat body cell. Digital images for display were imported into Photoshop (Adobe) and adjusted for gain, contrast, and settings.

Mouse strains

C57BL/6 mice were used for all studies. The generation of GFP-LC3 transgenic (Mizushima et al., 2004) and STING^{-/-} mice was described before, respectively (Liang et al., 2017). All animals were group-housed (one to five mice per cage) in a barrier facility at 23°C and provided Harlan Teklad chow diet and water ad libitum. Animal experiments being performed are approved by the University of Texas Southwestern Medical Center and Shanghai Jiaotong University School of Medicine (SHSMU), Institutional Animal Care and Use Committee.

Acute mouse exercise studies

Male mice aged 8–12-wk-old (WT, STING^{-/-}) were acclimated on a 10° uphill Exer 3/6 open treadmill (Columbus Instruments) for 2 d. Mice ran for 5 min at 8 m/min on day 1, and on day 2 mice ran for 5 min at 8 m/min and then another 5 min at 10 m/min. On day 3, mice were allowed to rest. On day 4, mice were subjected to a single bout of running starting at a speed of 10 m/min for 40 min. After 40 min, the treadmill speed was increased at a rate of 1 m/min every 10 min for a total of 30 min and then increased at the rate of 1 m/min every 5 min until reaching 90 min (for recording of electrical shock accounts) or 95 min (for all tissue collection and blood tests) or mice exhaustion (for maximum running distance). Exhaustion point was defined as more than 5 s mice spent on the electric shocker without resuming running. The total running time and distance were recorded for each mouse.

Mouse metabolic analysis

Blood chemistry

Serum TG and cholesterol were measured using the Chemistry Analyzer (Rayto Chemray800). Serum lactate, FFA, glycerol, insulin, and IL-13 were measured using the LD assay kit (A019-2; Nanjing Jiancheng), NEFA assay kit (A042-2-1; Nanjing Jiancheng), glycerol content assay kit (F005-1-1; Nanjing Jiancheng), mouse insulin ELISA Kit (CSB-E05071m; CUSABIO), and mouse IL-13 ELISA Kit (EK213/2; Multi Sciences), respectively.

Measurement of liver and muscle TG

Mouse gastrocnemius muscle and liver tissue were freshly collected and snap-frozen in liquid nitrogen. Then the TG content

was measured using a TG assay kit (A110-1; Nanjing Jiancheng) following the manufacturer's protocol.

Measurement of liver and muscle glycogen

Mouse thigh muscles were homogenized with 10 ml/mg double-distilled H₂O using an Ultra-Turrax tissue distintegrator and the samples were then placed on a 95°C-heat block for 15 min to inactivate enzymes in the samples. After centrifugation (18,000 *g*, 10 min at 4°C), 1 μ l liver sample supernatant or 6 μ l thigh muscle sample supernatant was used for the measurement of glycogen content using a Glycogen Assay kit (ab65620; Abcam).

Lipolysis assay

Fresh epididymal WAT (eWAT) was isolated from mice and cut into pieces (~50 mg per piece), followed by incubation in 1 ml serum-free medium containing 1% fatty acid-free BSA for 4 h. Glycerol release was measured using a free glycerol reagent (F6428; Sigma-Aldrich) and a glycerol standard (7793; Sigma-Aldrich), and free fatty acid release was measured using a Free Fatty Acid Quantification Colorimetric/Fluorometric Kit (K612; Biovision).

Fatty acid β -oxidation analysis

Frozen mouse gastrocnemius muscle was homogenized in 80% acetonitrile with 10 ml/mg tissue. After centrifugation (18,000 *g*, 10 min at 4°C), the supernatant of the sample was used for spectrometry analysis immediately. Liquid chromatography-mass spectrometry (LC-MS) was performed on an Agilent 1290 UHPLC system equipped with a binary solvent delivery manager, an auto sampler, and a column oven, coupled with a 6545 Quadrupole Time of Flight Mass Spectrometer with an electrospray interface (Agilent Technologies). The samples were extracted with protein precipitation as described above and separated with reverse-phase chromatography. The raw data were acquired in full scan positive mode within a mass range of *m/z* 100–1,000 with real-time mass calibration. Each mass response was corrected with the response of the respective internal standard. Each peak area ratio was used for relative quantitation. The data were processed with Mass Hunter software (Agilent Technologies).

CLAMS and body composition analysis

A comprehensive laboratory animal monitoring system (CLAMS; The Columbus Instruments) was used to simultaneously measure a series of metabolic parameters including energy

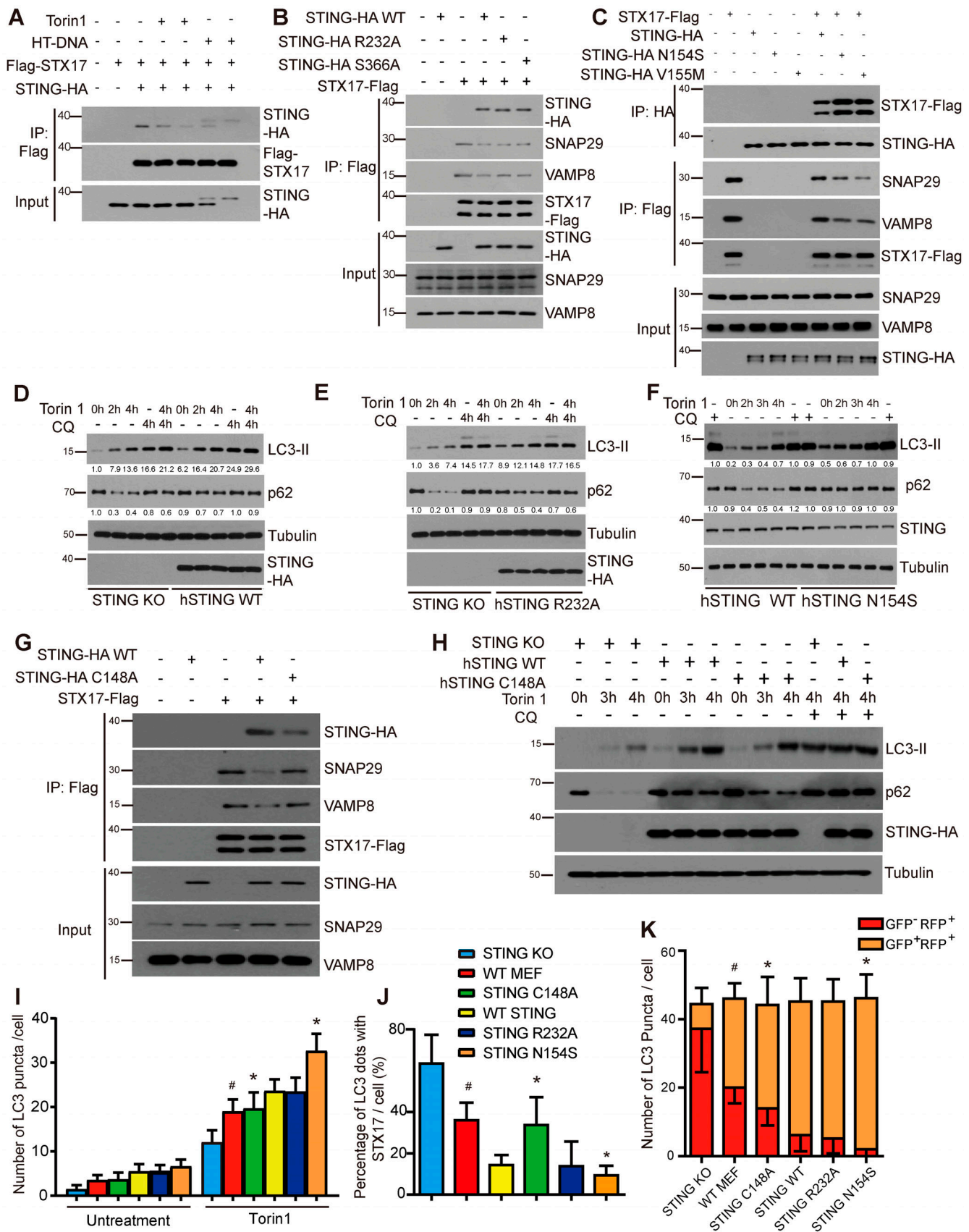


Figure 9. **Effect of STING mutations on autophagy regulation.** (A) MEFs stably expressing STING-HA and Flag-STX17 were treated with Torin 1 for 2 and 4 h or HT-DNA for 3 and 5 h, respectively, then the cells were lysed for immunoprecipitation and immunoblotting with indicated antibodies. (B) STING R232A

and STING S366A mutants disrupt STX17–SNAP29–VAMP8 SNAREpin assembly via their interaction with STX17. HEK293T cells were transfected with empty vector, STING-HA WT, STING-HA R232A, STING-HA S366A with or without STX17-Flag. 24 h after transfection, cells were lysed and immunoprecipitated with anti-Flag antibody. Immunoblotting was performed with indicated antibodies. **(C)** Enhanced interaction of STX17 with STING N154S and STING V155M further disrupts STX17–SNAP29–VAMP8 SNAREpin assembly. HEK293T cells were transfected with empty vector, STING-HA WT, STING-HA N153S, or STING-HA V155M with or without STX17-Flag. 24 h after transfection, cells were lysed and immunoprecipitated with anti-Flag antibody or anti-HA antibody. Immunoblotting was performed with the indicated antibodies. **(D–F)** Complementation of STING-KO MEFs with STING corrects their autophagy phenotypes. STING-KO and STING-KO MEFs complemented with HA-tagged STING WT (D), R223A mutant (E), or N154S mutant (F) were treated with Torin 1 with or without CQ for the indicated time. Immunoblotting was performed with indicated antibodies. Normalized fold change of LC3II Tubulin or p62/Tubulin was listed. **(G)** STING C148A mutant is defective for STX17 binding. HEK293T cells were transfected with empty vector, STING-HA WT, or STING-HA C148A with or without STX17-Flag. 24 h after transfection, cells were lysed and immunoprecipitated with anti-Flag antibody. Immunoblotting was performed with indicated antibodies. **(H)** STING-KO MEFs stably expressing STING-HA WT or STING-HA C148A mutant were treated with Torin 1 combined with or without CQ for the indicated time. Immunoblotting was performed with the indicated antibodies. **(I)** Quantification of the results in Fig. S4 E. Number of LC3 dots per cell. Data are mean \pm SD for 100 cells. * indicates the comparison with STING WT, $P \leq 0.001$. # indicates the comparison with STING KO, $P \leq 0.001$. **(J)** Quantification of the results in Fig. S5. Percentage of LC3 dots with STX17. Data are mean \pm SD for 100 cells. * indicates the comparison with STING WT, $P \leq 0.001$. # indicates the comparison with STING KO, $P \leq 0.001$. **(K)** Quantification of the results in Fig. S6. Quantitative analysis of acidified autophagosomes (GFP⁺RFP⁺) versus neutral autophagosomes (GFP⁺RFP⁻) per cell. Data are mean \pm SD for 100 cells. * indicates the comparison of RFP number with STING WT, $P \leq 0.001$. # indicates the comparison of RFP number with STING KO, $P \leq 0.001$. Source data are available for this figure: SourceData F9.

expenditure (heat production), oxygen consumption (VO_2), carbon dioxide production (VCO_2), respiratory exchange ratio, locomotor activity levels, and food intake over a 72-h period. Data were collected every 16 min. Fat mass and lean tissue mass were determined using the EchoMRI body composition analyzer (E26-245-M).

Histological analysis

For periodic acid–Schiff (PAS) staining, fresh tissues were immediately embedded in the OCT compound, cut into 10-mm sections, and stained with PAS staining kit (G1008; Servicebio). For Oil-Red staining, fresh tissues were immediately embedded in the OCT compound, cut into 10-mm sections, and stained with Oil-Red staining kit (G1016; Servicebio). The histological slides were obtained by an Olympus IX51 microscopy using a 20 \times (NA 0.75) lens at RT. Confocal images were obtained by an Olympus IX-83 confocal microscopy under RT using a 40 \times (NA 1.3) oil lens at RT. The colocalization analysis was performed by Image J Software.

Statistical analysis

Immunoblot signals were quantified using ImageJ. Statistical analysis was carried out using GraphPad (v8.0.1). Data of mammalian cells and animal experiments were evaluated by two-tailed unpaired Student's test and represented as mean \pm SEM, with a P value of < 0.05 being considered significant. We used two-way ANOVA model to test whether the effect of exercise in KO group is significantly different from that in WT group. If the P value of the interaction term (between gene KO and exercise) is < 0.05 , then we conclude that the gene KO significantly modifies the effect of exercise.

For fly data, statistical significance was determined in Prism using one-way ANOVA for multiple comparisons, followed by Tukey's test. All bar graphs resulting from these analyses show means \pm SD. For quantifications of fluorescence images, at least three independent experiments were used. P -values < 0.05 are considered significant and values are indicated with * (≤ 0.05), ** (≤ 0.01), *** (≤ 0.001), or **** (≤ 0.0001). Data distribution was assumed to be normal, but this was not formally tested.

Online supplemental material

Fig. S1 confirms that STING KO in mice did not affect the circular metabolic index, nor morphology of adipose tissue, skeleton muscle, as well as liver and fatty acid metabolism, compared with WT mice. Fig. S2 shows that STING has no influence on autophagosome initiation and canonical autophagy regulator upon energy stress. Fig. S3 shows that STING did not interact with YKT6, and STX17 translocation from ER depends on STING, while STING–SXT17 disassociation depends on energy crisis. Fig. S4 contains the identification of binding site of STING for STX17 and effects of STING mutants on autophagy initiation. Fig. S5 presents the analysis of STING and STING mutants in blocking the translocation of STX17 to autophagosome. Fig. S6 shows the functional analysis of STING mutants in autophagosome maturation.

Acknowledgments

We thank Yiru Huang (Southern Medical University, Guangzhou, China) and Tiemin Liu (Fudan University, Shanghai, China) for technical advice and assistance. We thank Professor Noboru Mizushima (Tokyo Medical and Dental University, Tokyo, Japan) for STX17 variant plasmids. We thank Michael Buszczak (UT Southwestern, Dallas, TX) for the dSting KO plasmids. We thank Xuemei Tong (SHSMU, Shanghai, China) for technical advice; Shuai Chen (Nanjing University, Nanjing, China) for technical advice and antibodies. We thank Yao Li (SHSMU) for help of mice maintenance, Jiqui Wang (SHSMU) for technical support of metabolic analysis, and Core facility of Basic Medical Science, Shanghai Jiaotong University School of Medicine for technical support of Q-TOF LC-MS analysis.

The work was supported in part by grants from NSFC (National Natural Science Foundation of China) (91754205, 91957204, 31771529, 31771523, 31801170, 31870830, 91854116, 32070741, and M-0140), Ministry of Science and Technology of the People's Republic of China (2019YFA0508602), Shanghai Science and Technology Commission (20JC1410100), Shanghai Municipal Science and Technology Project (20JC1411100), Shanghai Frontiers Science Center of Cellular Homeostasis and Human Diseases, and National Institutes of Health (RO1EY010199).

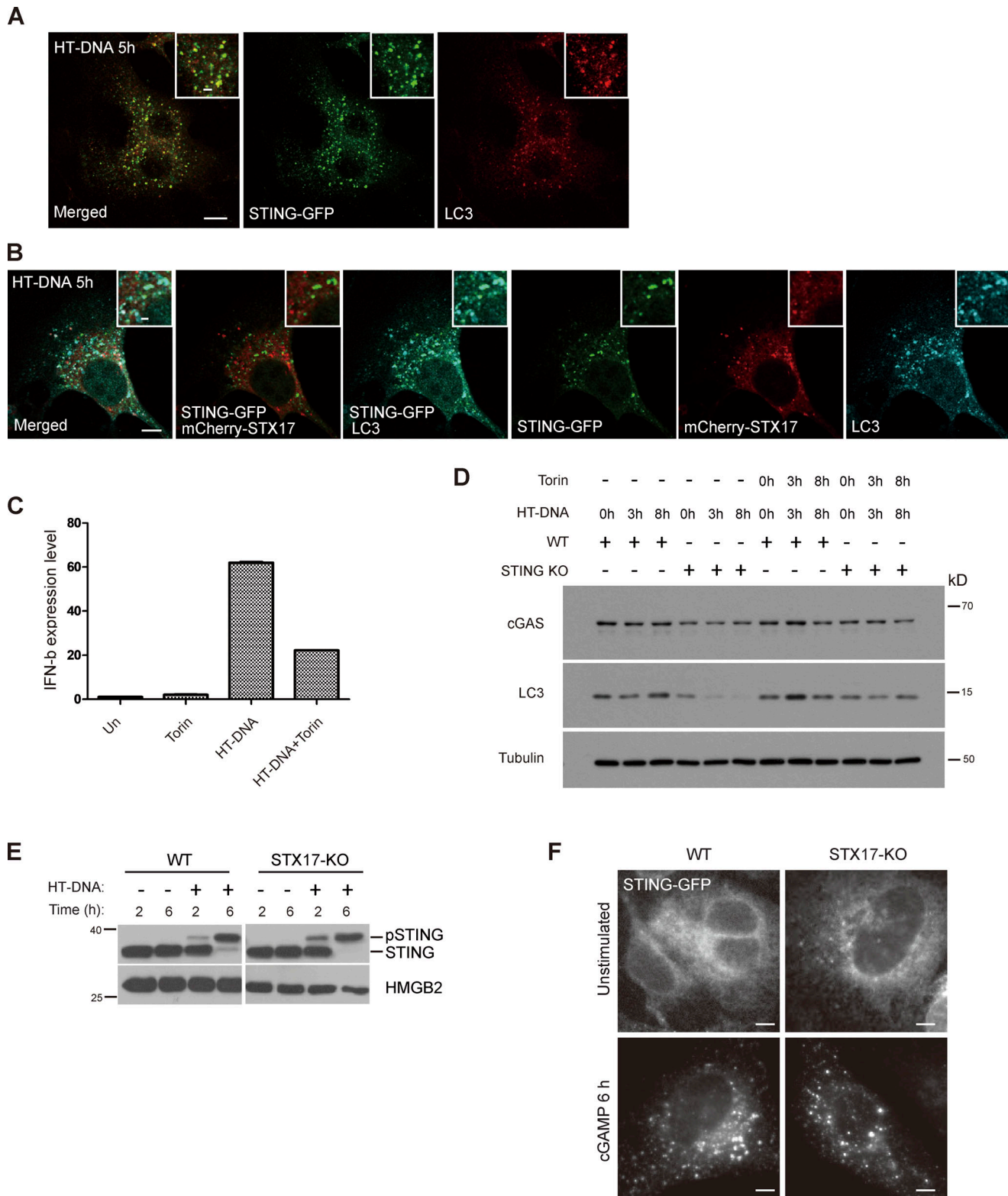


Figure 10. **STX17 and STING translocate to different types of autophagic vacuoles upon DNA stimulation.** (A) LC3 is recruited to STING positive vesicles. MEFs stably expressing STING-GFP was treated with HT-DNA for 5 h and stained with GFP and LC3 antibody. Scale bar for large images, 5 μ m; Scale bar for inset images, 1 μ m. (B) STX17 translocates to STING negative but LC3 positive vesicles. MEFs stably expressing STING-GFP and mCherry-STX17 were treated with HT-DNA for 5 h and stained with GFP, mCherry, and LC3 antibody. Scale bar for large images, 5 μ m; Scale bar for inset images, 1 μ m. (C) mTOR inhibition negatively regulates DNA-induced IFN β expression. WT cells were treated with Torin 1, HT-DNA, or HT-DNA plus Torin 1 for 5 h, and the indicated RNAs was extracted for qPCR. (D) STING mediates HT-DNA-induced autophagic response. WT and STING-KO MEFs were treated with HT-DNA or HT-DNA with Torin 1 for 3 or 8 h. Cells were lysed and analyzed for immunoblotting with indicated antibodies. (E) STX17 is not required for STING degradation. WT and

STX17 knock out cells were treated with HT-DNA for 2 or 6 h. Cells were collected for immunoblotting with the indicated antibodies. (F) STING translocates to vesicles upon cGAMP stimulation. WT and STX17 knock out cells stably expressing STING-GFP were treated with cGAMP for 6 h and then fixed for immunostaining. Scale bar, 5 μ m. Source data are available for this figure: SourceData F10.

The work was also sponsored by Program of Shanghai Subject Chief Scientist (19XD1402200) and supported by innovative research team of high-level local universities in Shanghai. (SHSMU-ZDCX20212000), Chinese Universities Scientific Fund and CAMS (Chinese Academy of Medical Sciences) Innovation Fund for Medical Sciences (2019-I2M-5-051).

The authors declare no competing financial interests.

Author contributions: Y. Rong and S. Zhang performed the most of biological and biochemical experiments characterizing STING function in mammalian cells and mice; N. Nandi performed analysis of loss of dSTING in *Drosophila*; L. Li, Y. Zhao, W. Yuan, Z. Wu, and C. Zhou helped with cell biology experiments; G. Xiao performed statistical analysis; Y. Liu and Y. Wei helped with the mouse experiments; B. Levine, S. Mou, N. Yan, L. Deng, Z. Tang, X. Liu, and H. Kramer helped to conceive the project; N. Yan provided the HT-DNA; Y. Rong and Q. Zhong designed the experiments, analyzed the data and wrote the manuscript with the help of all authors.

Submitted: 11 February 2022

Revised: 7 March 2022

Accepted: 8 March 2022

References

- Arasaki, K., H. Shimizu, H. Mogari, N. Nishida, N. Hirota, A. Furuno, Y. Kudo, M. Baba, N. Baba, J. Cheng, et al. 2015. A role for the ancient SNARE syntaxin 17 in regulating mitochondrial division. *Dev. Cell.* 32:304–317. <https://doi.org/10.1016/j.devcel.2014.12.011>
- Bas, L., D. Papinski, M. Licheva, R. Torggler, S. Rohringer, M. Schuschnig, and C. Kraft. 2018. Reconstitution reveals Ykt6 as the autophagosomal SNARE in autophagosome-vacuole fusion. *J. Cell Biol.* 217:3656–3669. <https://doi.org/10.1083/jcb.201804028>
- Bernet, J.D., J.D. Doles, J.K. Hall, K. Kelly Tanaka, T.A. Carter, and B.B. Olwin. 2014. p38 MAPK signaling underlies a cell-autonomous loss of stem cell self-renewal in skeletal muscle of aged mice. *Nat. Med.* 20:265–271. <https://doi.org/10.1038/nm.3465>
- Blanc, R.S., J.G. Kallenbach, J.F. Bachman, A. Mitchell, N.D. Paris, and J.V. Chakkalakal. 2020. Inhibition of inflammatory CCR2 signaling promotes aged muscle regeneration and strength recovery after injury. *Nat. Commun.* 11:4167. <https://doi.org/10.1038/s41467-020-17620-8>
- Burdette, D.L., K.M. Monroe, K. Sotelo-Troha, J.S. Iwig, B. Eckert, M. Hyodo, Y. Hayakawa, and R.E. Vance. 2011. STING is a direct innate immune sensor of cyclic di-GMP. *Nature.* 478:515–518. <https://doi.org/10.1038/nature10429>
- Cai, X., Y.-H. Chiu, and Z.J. Chen. 2014. The cGAS-cGAMP-STING pathway of cytosolic DNA sensing and signaling. *Mol. Cell.* 54:289–296. <https://doi.org/10.1016/j.molcel.2014.03.040>
- Chen, M., Q. Meng, Y. Qin, P. Liang, P. Tan, L. He, Y. Zhou, Y. Chen, J. Huang, R.F. Wang, and J. Cui. 2016. TRIM14 inhibits cGAS degradation mediated by selective autophagy receptor p62 to promote innate immune responses. *Mol. Cell.* 64:105–119. <https://doi.org/10.1016/j.molcel.2016.08.025>
- Chu, T.T., X. Tu, K. Yang, J. Wu, J.J. Repa, and N. Yan. 2021. Tonic prime-boost of STING signalling mediates Niemann-Pick disease type C. *Nature.* 596:570–575. <https://doi.org/10.1038/s41586-021-03762-2>
- Diao, J., R. Liu, Y. Rong, M. Zhao, J. Zhang, Y. Lai, Q. Zhou, L.M. Wilz, J. Li, S. Vivona, et al. 2015. ATG14 promotes membrane tethering and fusion of autophagosomes to endolysosomes. *Nature.* 520:563–566. <https://doi.org/10.1038/nature14147>
- Dobbs, N., N. Burnaevskiy, D. Chen, V.K. Gonugunta, N.M. Alto, and N. Yan. 2015. STING activation by translocation from the ER is associated with infection and autoinflammatory disease. *Cell Host Microbe.* 18:157–168. <https://doi.org/10.1016/j.chom.2015.07.001>
- Eaglesham, J.B., Y. Pan, T.S. Kupper, and P.J. Kranzusch. 2019. Viral and metazoan poxins are cGAMP-specific nucleases that restrict cGAS-STING signalling. *Nature.* 566:259–263. <https://doi.org/10.1038/s41586-019-0928-6>
- Gao, J., F. Reggiori, and C. Ungermann. 2018. A novel in vitro assay reveals SNARE topology and the role of Ykt6 in autophagosome fusion with vacuoles. *J. Cell Biol.* 217:3670–3682. <https://doi.org/10.1083/jcb.201804039>
- Gkirtzimanaki, K., E. Kabrani, D. Nikoleri, A. Polyzos, A. Blanas, P. Sidiropoulos, A. Makriganakis, G. Bertias, D.T. Boumpas, and P. Verginis. 2018. IFN α impairs autophagic degradation of mtDNA promoting autoreactivity of SLE monocytes in a STING-dependent fashion. *Cell Rep.* 25:921–933.e5. <https://doi.org/10.1016/j.celrep.2018.09.001>
- Gonugunta, V.K., T. Sakai, V. Pokatayev, K. Yang, J. Wu, N. Dobbs, and N. Yan. 2017. Trafficking-mediated STING degradation requires sorting to acidified endolysosomes and can be targeted to enhance anti-tumor response. *Cell Rep.* 21:3234–3242. <https://doi.org/10.1016/j.celrep.2017.11.061>
- Goodman, A.G., B.M. Kitay, K. Konno, R.G. Zhai, and G.N. Barber. 2013. Evolutionary conservation of STING, an innate immune effector and DNA sensor, in *Drosophila melanogaster*. *Cytokine.* 63:266. <https://doi.org/10.1016/j.cyto.2013.06.099>
- Gratz, S.J., M.M. Harrison, J. Wildonger, and K.M. O'Connor-Giles. 2015. Precise genome editing of *Drosophila* with CRISPR RNA-guided Cas9. *Methods Mol. Biol.* 1311:335–348. https://doi.org/10.1007/978-1-4939-2687-9_22
- Gui, X., H. Yang, T. Li, X. Tan, P. Shi, M. Li, F. Du, and Z.J. Chen. 2019. Autophagy induction via STING trafficking is a primordial function of the cGAS pathway. *Nature.* 567:262–266. <https://doi.org/10.1038/s41586-019-1006-9>
- Hamasaki, M., N. Furuta, A. Matsuda, A. Nezu, A. Yamamoto, N. Fujita, H. Oomori, T. Noda, T. Haraguchi, Y. Hiraoka, et al. 2013. Autophagosomes form at ER-mitochondria contact sites. *Nature.* 495:389–393. <https://doi.org/10.1038/nature11910>
- He, C., M.C. Bassik, V. Moresi, K. Sun, Y. Wei, Z. Zou, Z. An, J. Loh, J. Fisher, Q. Sun, et al. 2012. Exercise-induced BCL2-regulated autophagy is required for muscle glucose homeostasis. *Nature.* 481:511–515. <https://doi.org/10.1038/nature10758>
- Ishikawa, H., and G.N. Barber. 2008. STING is an endoplasmic reticulum adaptor that facilitates innate immune signalling. *Nature.* 455:674–678. <https://doi.org/10.1038/nature07317>
- Ishikawa, H., Z. Ma, and G.N. Barber. 2009. STING regulates intracellular DNA-mediated, type I interferon-dependent innate immunity. *Nature.* 461:788–792. <https://doi.org/10.1038/nature08476>
- Itakura, E., C. Kishi-Itakura, and N. Mizushima. 2012. The hairpin-type tail-anchored SNARE syntaxin 17 targets to autophagosomes for fusion with endosomes/lysosomes. *Cell.* 151:1256–1269. <https://doi.org/10.1016/j.cell.2012.11.001>
- Jeremiah, N., B. Neven, M. Gentili, I. Callebaut, S. Maschalidi, M.C. Stolzenberg, N. Goudin, M.L. Fremont, P. Nitschke, T.J. Molina, et al. 2014. Inherited STING-activating mutation underlies a familial inflammatory syndrome with lupus-like manifestations. *J. Clin. Invest.* 124:5516–5520. <https://doi.org/10.1172/JCI79100>
- Jiang, P., T. Nishimura, Y. Sakamaki, E. Itakura, T. Hatta, T. Natsume, and N. Mizushima. 2014. The HOPS complex mediates autophagosome-lysosome fusion through interaction with syntaxin 17. *Mol. Biol. Cell.* 25:1327–1337. <https://doi.org/10.1091/mbc.E13-08-0447>
- Jin, L., P.M. Waterman, K.R. Jonscher, C.M. Short, N.A. Reisdorph, and J.C. Cambier. 2008. MPYS, a novel membrane tetraspanner, is associated with major histocompatibility complex class II and mediates transduction of apoptotic signals. *Mol. Cell Biol.* 28:5014–5026. <https://doi.org/10.1128/MCB.00640-08>
- Kumar, S., Y. Gu, Y.P. Abudu, J.A. Bruun, A. Jain, F. Farzam, M. Mudd, J.H. Anonsen, T.E. Rusten, G. Kasof, et al. 2019. Phosphorylation of syntaxin 17 by TBK1 controls autophagy initiation. *Dev. Cell.* 49:130–144.e6. <https://doi.org/10.1016/j.devcel.2019.01.027>

- Kumar, S., R. Javed, M. Mudd, S. Pallikkuth, K.A. Lidke, A. Jain, K. Tangavelou, S.R. Gudmundsson, C. Ye, T.E. Rusten, et al. 2021. Mammalian hybrid pre-autophagosomal structure HyPAS generates autophagosomes. *Cell*. 184:5950–5969.e22. <https://doi.org/10.1016/j.cell.2021.10.017>
- Levine, B., and G. Kroemer. 2019. Biological functions of autophagy genes: A disease perspective. *Cell*. 176:11–42. <https://doi.org/10.1016/j.cell.2018.09.048>
- Levine, B., N. Mizushima, and H.W. Virgin. 2011. Autophagy in immunity and inflammation. *Nature*. 469:323–335. <https://doi.org/10.1038/nature09782>
- Liang, H., L. Deng, Y. Hou, X. Meng, X. Huang, E. Rao, W. Zheng, H. Mauceri, M. Mack, M. Xu, et al. 2017. Host STING-dependent MDSC mobilization drives extrinsic radiation resistance. *Nat. Commun.* 8:1736. <https://doi.org/10.1038/s41467-017-01566-5>
- Liang, Q., G.J. Seo, Y.J. Choi, M.J. Kwak, J. Ge, M.A. Rodgers, M. Shi, B.J. Leslie, K.P. Hopfner, T. Ha, et al. 2014. Crosstalk between the cGAS DNA sensor and Beclin-1 autophagy protein shapes innate antimicrobial immune responses. *Cell Host Microbe*. 15:228–238. <https://doi.org/10.1016/j.chom.2014.01.009>
- Liu, D., H. Wu, C. Wang, Y. Li, H. Tian, S. Siraj, S.A. Sehgal, X. Wang, J. Wang, Y. Shang, et al. 2019. STING directly activates autophagy to tune the innate immune response. *Cell Death Differ.* 26:1735–1749. <https://doi.org/10.1038/s41418-018-0251-z>
- Liu, Y., A.A. Jesus, B. Marrero, D. Yang, S.E. Ramsey, G.A. Montealegre Sanchez, K. Tenbrock, H. Wittkowski, O.Y. Jones, H.S. Kuehn, et al. 2014. Activated STING in a vascular and pulmonary syndrome. *N. Engl. J. Med.* 371:507–518. <https://doi.org/10.1056/nejmoal312625>
- Liu, Y., P.T. Nguyen, X. Wang, Y. Zhao, C.E. Meacham, Z. Zou, B. Bordieanu, M. Johanns, D. Vertommen, T. Wijshake, et al. 2020. TLR9 and beclin 1 crosstalk regulates muscle AMPK activation in exercise. *Nature*. 578:605–609. <https://doi.org/10.1038/s41586-020-1992-7>
- Low, P., A. Varga, K. Piracs, P. Nagy, Z. Szatmari, M. Sass, and G. Juhasz. 2013. Impaired proteasomal degradation enhances autophagy via hypoxia signaling in *Drosophila*. *BMC Cell Biol.* 14:29. <https://doi.org/10.1186/1471-2121-14-29>
- Matsui, T., P. Jiang, S. Nakano, Y. Sakamaki, H. Yamamoto, and N. Mizushima. 2018. Autophagosomal YKT6 is required for fusion with lysosomes independently of syntaxin 17. *J. Cell Biol.* 217:2633–2645. <https://doi.org/10.1083/jcb.201712058>
- Mizushima, N.. 2007. Autophagy: Process and function. *Genes Dev.* 21:2861–2873. <https://doi.org/10.1101/gad.1599207>
- Mizushima, N., T. Matsui, and H. Yamamoto. 2019. YKT6 as a second SNARE protein of mammalian autophagosomes. *Autophagy*. 15:176–177. <https://doi.org/10.1080/15548627.2018.1532262>
- Mizushima, N., A. Yamamoto, M. Matsui, T. Yoshimori, and Y. Ohsumi. 2004. In vivo analysis of autophagy in response to nutrient starvation using transgenic mice expressing a fluorescent autophagosome marker. *Mol. Biol. Cell*. 15:1101–1111. <https://doi.org/10.1091/mbc.e03-09-0704>
- Moretti, J., S. Roy, D. Bozec, J. Martinez, J.R. Chapman, B. Ueberheide, D.W. Lamming, Z.J. Chen, T. Horng, G. Yeretssian, et al. 2017. STING senses microbial viability to orchestrate stress-mediated autophagy of the endoplasmic reticulum. *Cell*. 171:809–823.e13. <https://doi.org/10.1016/j.cell.2017.09.034>
- Nandi, N., L.K. Tyra, D. Stenesen, and H. Kramer. 2017. Stress-induced Cdk5 activity enhances cytoprotective basal autophagy in *Drosophila melanogaster* by phosphorylating acinus at serine⁴³⁷. *Elife*. 6:e30760. <https://doi.org/10.7554/eLife.30760>
- Pulipparacharuvil, S., M.A. Akbar, S. Ray, E.A. Sevrioukov, A.S. Haberman, J. Rohrer, and H. Kramer. 2005. *Drosophila* Vps16A is required for trafficking to lysosomes and biogenesis of pigment granules. *J. Cell Sci.* 118:3663–3673. <https://doi.org/10.1242/jcs.02502>
- Roach, W.G., J.A. Chavez, C.P. Miinea, and G.E. Lienhard. 2007. Substrate specificity and effect on GLUT4 translocation of the Rab GTPase-activating protein Tbc1d1. *Biochem. J.* 403:353–358. <https://doi.org/10.1042/BJ20061798>
- Saitoh, T., N. Fujita, T. Hayashi, K. Takahara, T. Satoh, H. Lee, K. Matsunaga, S. Kageyama, H. Omori, T. Noda, et al. 2009. Atg9a controls dsDNA-driven dynamic translocation of STING and the innate immune response. *Proc. Natl. Acad. Sci. USA*. 106:20842–20846. <https://doi.org/10.1073/pnas.0911267106>
- Saleeb, R.S., D.M. Kavanagh, A.R. Dun, P.A. Dalgarno, and R.R. Duncan. 2019. A VPS33A-binding motif on syntaxin 17 controls autophagy completion in mammalian cells. *J. Biol. Chem.* 294:4188–4201. <https://doi.org/10.1074/jbc.RA118.005947>
- Shang, G., C. Zhang, Z.J. Chen, X.C. Bai, and X. Zhang. 2019. Cryo-EM structures of STING reveal its mechanism of activation by cyclic GMP-AMP. *Nature*. 567:389–393. <https://doi.org/10.1038/s41586-019-0998-5>
- Simonson, D.C., and R.A. DeFronzo. 1990. Indirect calorimetry: Methodological and interpretative problems. *Am. J. Physiol.* 258:E399–E412. <https://doi.org/10.1152/ajpendo.1990.258.3.E399>
- Sliter, D.A., J. Martinez, L. Hao, X. Chen, N. Sun, T.D. Fischer, J.L. Burman, Y. Li, Z. Zhang, D.P. Narendra, et al. 2018. Parkin and PINK1 mitigate STING-induced inflammation. *Nature*. 561:258–262. <https://doi.org/10.1038/s41586-018-0448-9>
- Sugo, M., H. Kimura, K. Arasaki, T. Amemiya, N. Hirota, N. Dohmae, Y. Imai, T. Inoshita, K. Shiba-Fukushima, N. Hattori, et al. 2018. Syntaxin 17 regulates the localization and function of PGAM5 in mitochondrial division and mitophagy. *EMBO J.* 37:e98899. <https://doi.org/10.15252/embj.201798899>
- Sui, H., M. Zhou, H. Imamichi, X. Jiao, B.T. Sherman, H.C. Lane, and T. Imamichi. 2017. STING is an essential mediator of the Ku70-mediated production of IFN-λ in response to exogenous DNA. *Sci. Signal.* 10:eah5054. <https://doi.org/10.1126/scisignal.aah5054>
- Sun, L., J. Wu, F. Du, X. Chen, and Z.J. Chen. 2013. Cyclic GMP-AMP synthase is a cytosolic DNA sensor that activates the type I interferon pathway. *Science*. 339:786–791. <https://doi.org/10.1126/science.1232458>
- Sun, W., Y. Li, L. Chen, H. Chen, F. You, X. Zhou, Y. Zhou, Z. Zhai, D. Chen, and Z. Jiang. 2009. ERIS, an endoplasmic reticulum IFN stimulator, activates innate immune signaling through dimerization. *Proc. Natl. Acad. Sci. USA*. 106:8653–8658. <https://doi.org/10.1073/pnas.0900850106>
- Takats, S., G. Glatz, G. Szenci, A. Boda, G.V. Horvath, K. Hegedus, A.L. Kovacs, and G. Juhasz. 2018. Non-canonical role of the SNARE protein Ykt6 in autophagosome-lysosome fusion. *PLoS Genet.* 14:e1007359. <https://doi.org/10.1371/journal.pgen.1007359>
- Takats, S., P. Nagy, A. Varga, K. Piracs, M. Karpati, K. Varga, A.L. Kovacs, K. Hegedus, and G. Juhasz. 2013. Autophagosomal Syntaxin17-dependent lysosomal degradation maintains neuronal function in *Drosophila*. *J. Cell Biol.* 201:531–539. <https://doi.org/10.1083/jcb.201211160>
- Tanaka, Y., and Z.J. Chen. 2012. STING specifies IRF3 phosphorylation by TBK1 in the cytosolic DNA signaling pathway. *Sci. Signal.* 5:ra20. <https://doi.org/10.1126/scisignal.2002521>
- Vats, S., and R. Manjithaya. 2019. A reversible autophagy inhibitor blocks autophagosome-lysosome fusion by preventing Stx17 loading onto autophagosomes. *Mol. Biol. Cell*. 30:2283–2295. <https://doi.org/10.1091/mbc.E18-08-0482>
- Wang, Y., L. Li, C. Hou, Y. Lai, J. Long, J. Liu, Q. Zhong, and J. Diao. 2016. SNARE-mediated membrane fusion in autophagy. *Semin. Cell Dev. Biol.* 60:97–104. <https://doi.org/10.1016/j.semcdb.2016.07.009>
- Watson, R.O., P.S. Manzanillo, and J.S. Cox. 2012. Extracellular M. tuberculosis DNA targets bacteria for autophagy by activating the host DNA-sensing pathway. *Cell*. 150:803–815. <https://doi.org/10.1016/j.cell.2012.06.040>
- Woodward, J.J., A.T. Iavarone, and D.A. Portnoy. 2010. c-di-AMP secreted by intracellular *Listeria monocytogenes* activates a host type I interferon response. *Science*. 328:1703–1705. <https://doi.org/10.1126/science.1189801>
- Wu, J.X., L. Sun, X. Chen, F. Du, H. Shi, C. Chen, and Z.J. Chen. 2013. Cyclic GMP-AMP is an endogenous second messenger in innate immune signaling by cytosolic DNA. *Science*. 339:826–830. <https://doi.org/10.1126/science.1229963>
- Wu, X.M., F.-H. Wu, X. Wang, L. Wang, J.N. Siedow, W. Zhang, and Z.-M. Pei. 2014. Molecular evolutionary and structural analysis of the cytosolic DNA sensor cGAS and STING. *Nucleic Acids Res.* 42:8243–8257. <https://doi.org/10.1093/nar/gku569>
- Zhang, X., H. Shi, J. Wu, X.W. Zhang, L. Sun, C. Chen, and Z.J. Chen. 2013. Cyclic GMP-AMP containing mixed phosphodiester linkages is an endogenous high-affinity ligand for STING. *Mol. Cell*. 51:226–235. <https://doi.org/10.1016/j.molcel.2013.05.022>
- Zhong, B., Y. Yang, S. Li, Y.-Y. Wang, Y. Li, F. Diao, C. Lei, X. He, L. Zhang, P. Tien, and H.-B. Shu. 2008. The adaptor protein MITA links virus-sensing receptors to IRF3 transcription factor activation. *Immunity*. 29:538–550. <https://doi.org/10.1016/j.immuni.2008.09.003>

Supplemental material

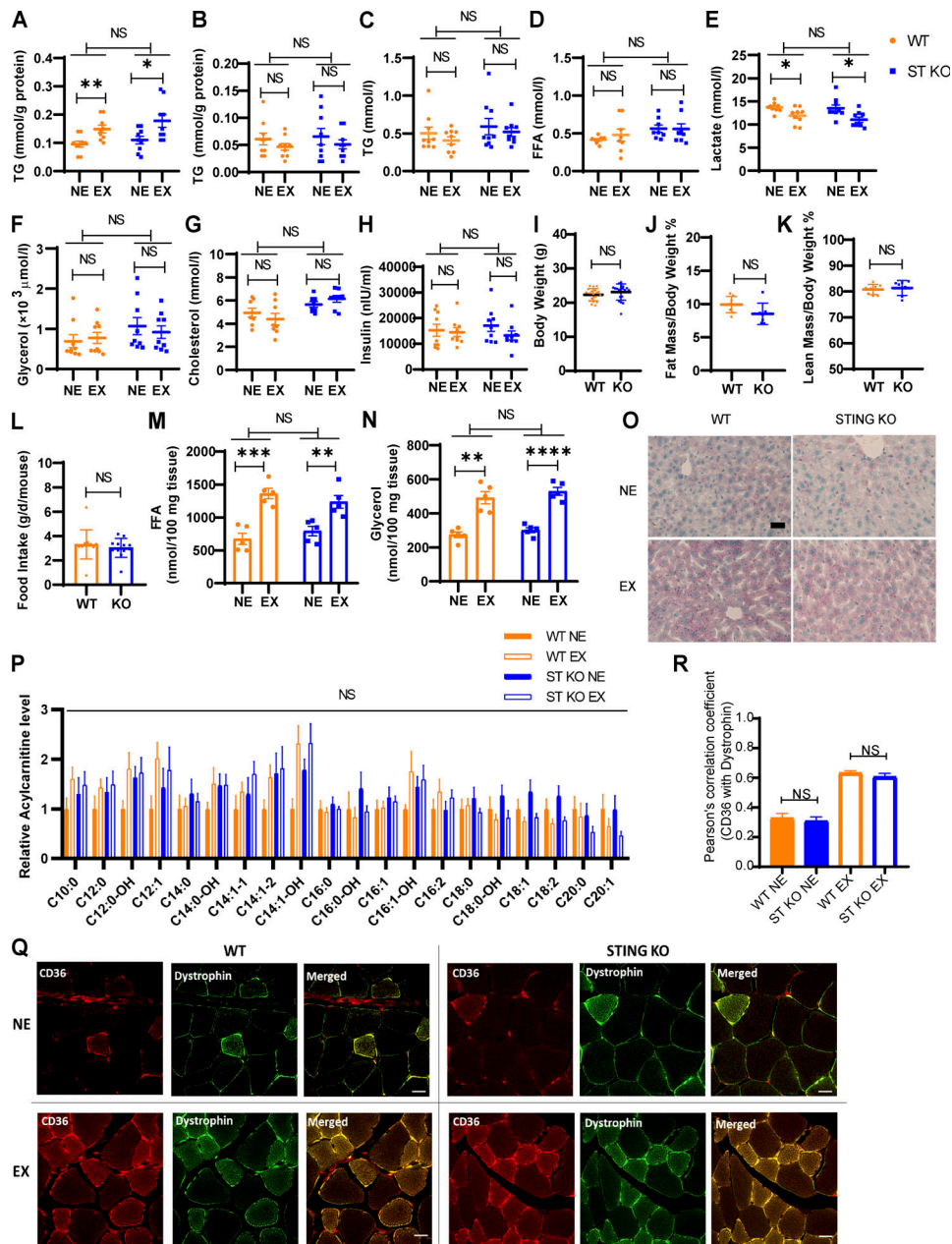


Figure S1. Metabolic index assessment, morphology characterization and fatty acid metabolism analysis of WT and STING KO mice. (A and B) Triglyceride (TG) content of livers (A) and gastrocnemius muscles (B) were measured in 8–12 wk old WT and STING KO mice ($n = 9$) before and after exercise. Serum biochemistry indexes were assessed in 8–12 wk old WT and STING KO mice before and after exercise. NS, not significant. Unpaired two-tailed T test for comparison of two groups. Two-way ANOVA for comparison of magnitude of changes between different genotypes in mice of different genotypes. **(C–H)** Serum TG (C; $n = 9$), serum FFA (D; $n = 9$), serum lactate (E; $n = 9$), serum glycerol (F; $n = 9$), serum cholesterol (G; $n = 9$), serum insulin (H; $n = 9$) were measured. NS, not significant; *, $P \leq 0.05$. Unpaired two-tailed t test for comparison of two groups. Two-way ANOVA for comparison of magnitude of changes between different groups in mice of different genotypes. **(I–L)** Body weight (I; $n = 18,19$), total fat mass (J; $n = 7$), total lean mass (K; $n = 7$) and food intake (L; $n = 11$), of 8–12 wk old mice with indicated genotypes were measured. Data are represented as mean \pm SEM. ST, STING; NE, non-exercise; EX, exercise. NS, not significant; *, $P \leq 0.05$; **, $P \leq 0.01$. Unpaired two-tailed t test for comparison of two groups. **(M and N)** Lipolysis activity in WT mice and STING KO mice. Ex vivo lipolysis assay for eWAT explants from 8–12 wk old WT and STING KO mice before and after exercise ($n = 5$). Free fatty acid (FFA; M) and glycerol release (N) were measured. Data are represented as mean \pm SEM. NS, not significant; **, $P \leq 0.01$; ***, $P \leq 0.001$; ****, $P \leq 0.0001$. Unpaired two-tailed t test for comparison of two groups. Two-way ANOVA for comparison of magnitude of changes between different groups in mice of different genotypes. **(O)** Representative images of Oil-Red staining in mice liver with indicated genotypes before and after exercise. Scale bar, 50 μm . **(P)** The relative metabolite abundance of long-chain acylcarnitines in WT and STING KO mice gastrocnemius muscles upon exercise or non-exercise ($n = 5$). NS, not significant. **(Q and R)** The translocation of CD36 to plasma membrane in STING KO mice after exercise. Representative images (Q) and quantification (R) of CD36 co-localization of Dystrophin in mice tibialis anterior muscles ($n = 4$) with indicated genotypes before and after exercise. Data are represented as mean \pm SEM. An area of 441 mm^2 per mouse was evaluated. ST, STING; NE, non-exercise; EX, exercise. NS, not significant, *, $P \leq 0.05$; **, $P \leq 0.01$; ***, $P \leq 0.001$; ****, $P \leq 0.0001$. Unpaired two-tailed t test for comparison of two groups. Two-way ANOVA for comparison of magnitude of changes between different groups in mice of different genotypes. Scale bar, 20 μm .

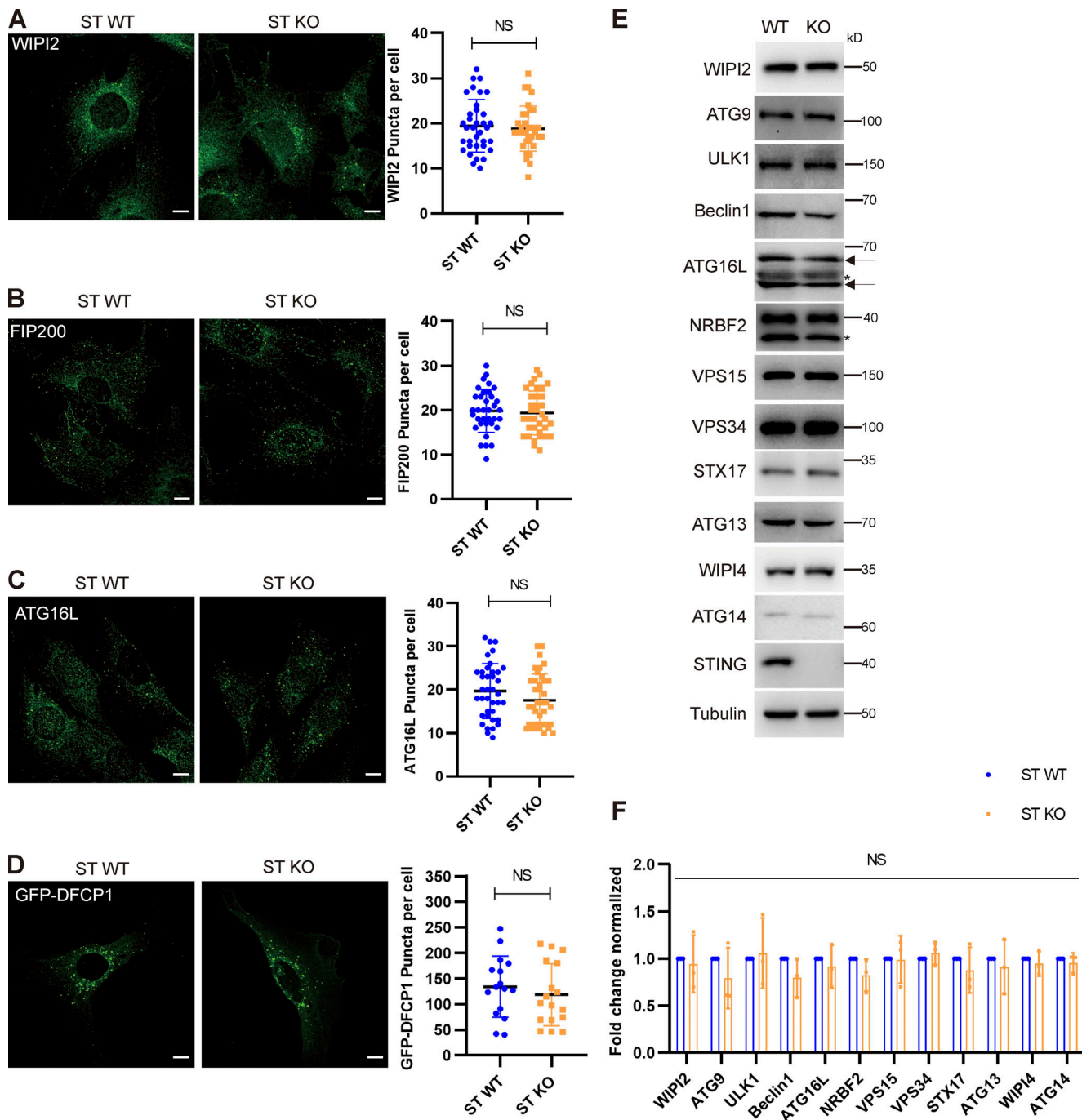


Figure S2. **STING has not influence on autophagosome initiation and canonical autophagy regulators.** (A–C) STING WT or KO MEF cells were treated with Torin 1 for 3 h before immunostaining by anti-WIPI2 (A), FIP200 (B), or ATG16L (C) primary antibodies and secondary antibodies. Images were taken by confocal microscopy. Representative images were shown on left panels. Right panels show the quantification of puncta number for the indicated proteins. Scale bar, 10 μ m. Data are represented as mean \pm SD for at least 30 cells. NS, not significant. Unpaired two-tailed *t* test for comparison of two groups. (D) STING WT and STING KO MEFs were transfected with GFP-DFCP1 for 24 h, then treated with Torin 1 for 3 h before fluorescence of GFP-DFCP1 was imaged by confocal microscopy. Representative images were shown on left panels. Right panels show the quantification of puncta number of the indicated proteins. Data are represented as mean \pm SD for at least 30 cells. NS, not significant. Unpaired two-tailed *t* test for comparison of two groups. (E) Canonical autophagy regulator expression level analysis in STING WT or STING KO MEF cells. STING WT and STING KO MEF cells were collected and lysed for Western blotting by the indicated antibodies. (F) Quantification of three independent repeats of E. Data are represented as mean \pm SD. NS, not significant; ST, STING. Unpaired two-tailed *t* test for comparison of two groups. Source data are available for this figure: SourceData FS2.

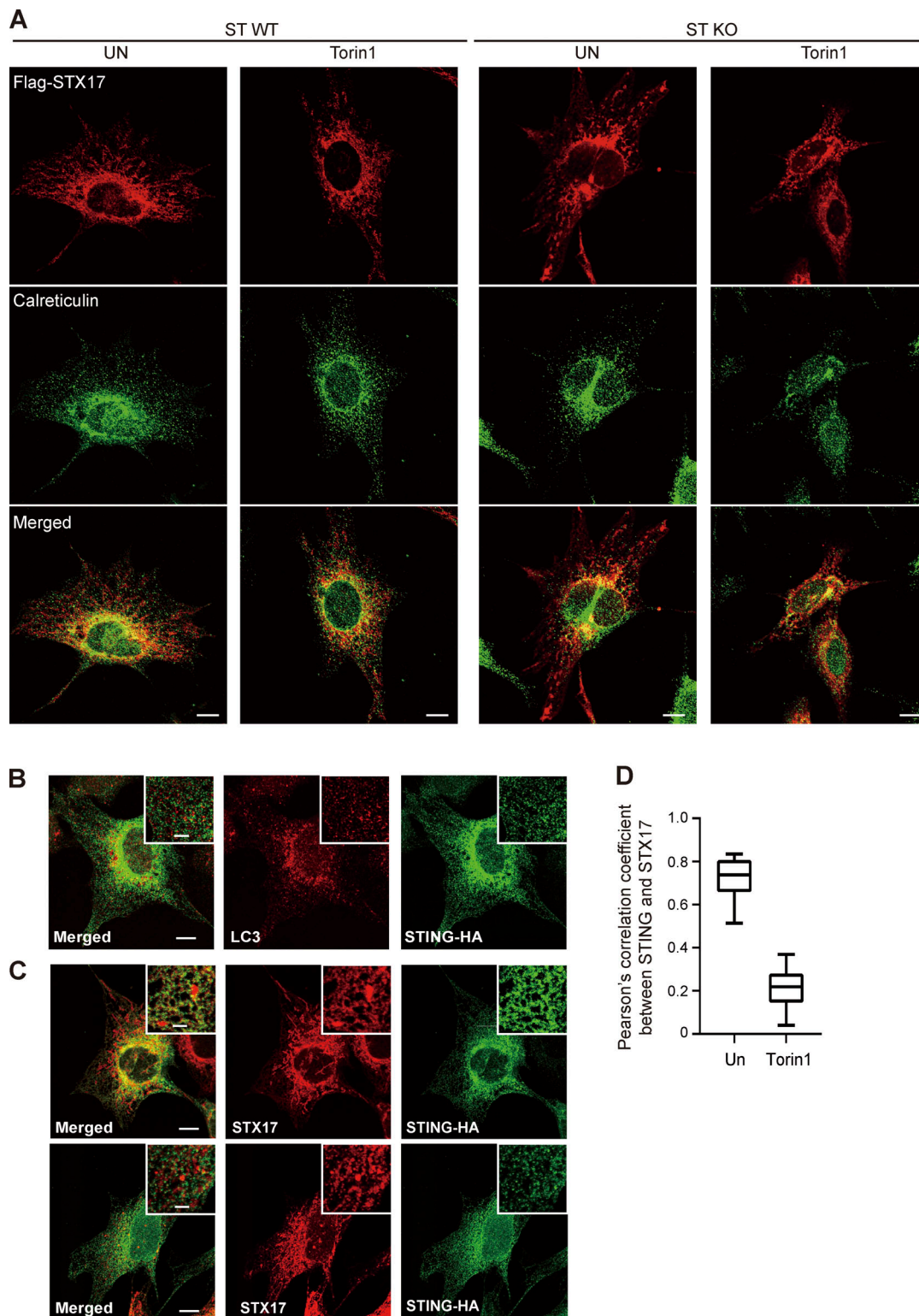


Figure S3. **STX17 translocation depends on STING, while STING-STX17 disassociation depends on energy crisis.** (A) Retention of STX17 on ER depends on STING. STING WT or STING KO cells were transfected with Flag-STX17. After 24 h of transfection, cells were treated with Torin 1 for 3 h or non-treatment. Then cells were fixed and stained by indicated antibodies and images were taken by confocal microscopy. Representative images were shown. Scale bar, 10 μ m. (B) STING does not translocate to autophagosomes during autophagy. MEFs stably expressing STING-HA were treated with Torin 1 for 3 h and then stained with indicated antibodies. Scale bar for large images, 5 μ m; scale bar for inset images, 1 μ m. (C) STING colocalizes with STX17 on ER but dissociates upon autophagic stress. MEFs stably expressing STING-HA and STX17-Flag stained with antibodies against HA and Flag without treatment (upper panel). MEFs stably expressing STING-HA were treated with Torin 1 for 3 h and then stained with antibodies against HA and LC3 (bottom panel). Scale bar for large images, 5 μ m; scale bar for inset images, 1 μ m. (D) Quantification of the colocalization between STING and STX17. Quantitative analysis of the colocalization between STING and STX17 in D. Data are mean \pm SEM for 30 cells.

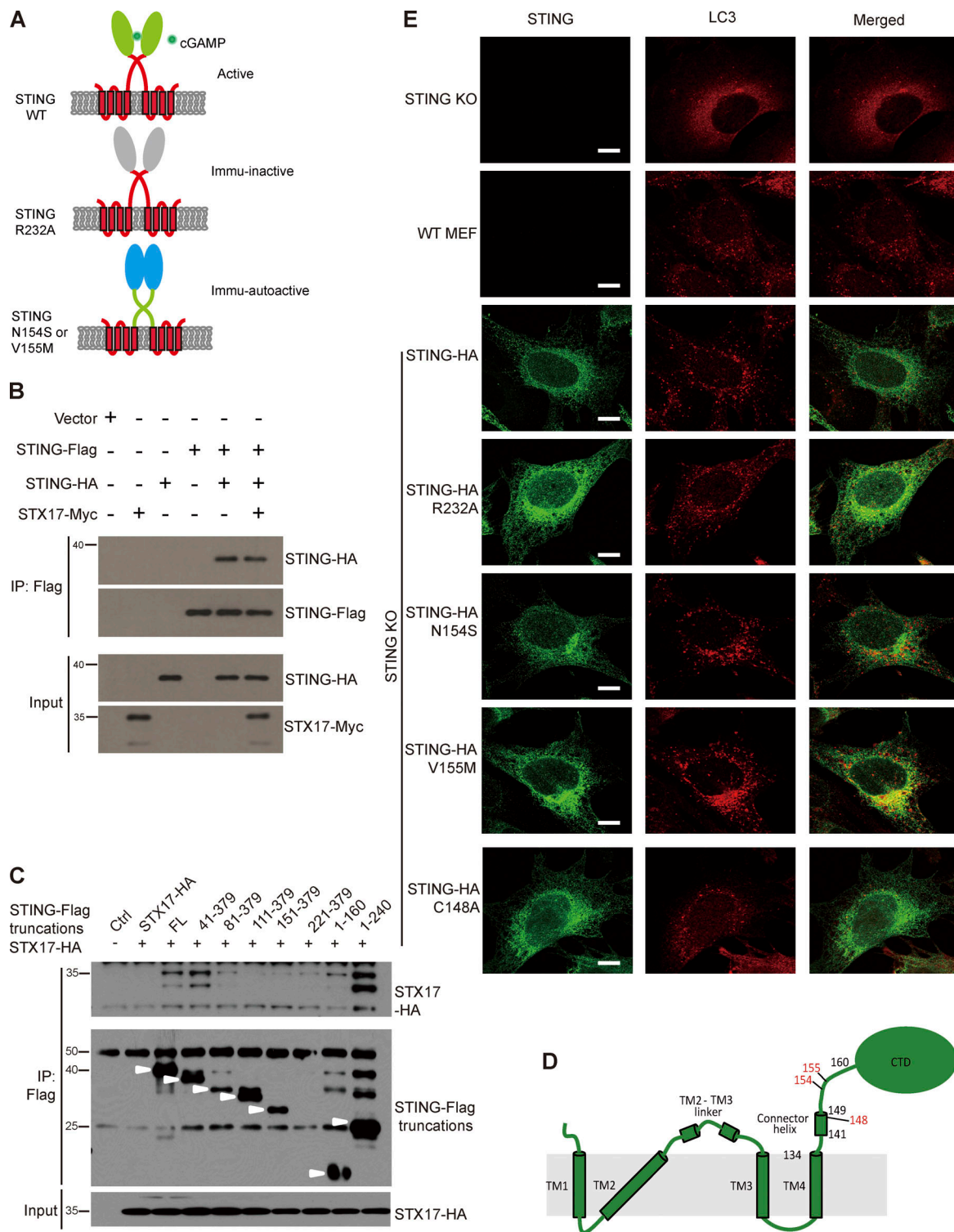


Figure S4. **Identifying the binding site of STING for STX17 and effects of STING mutants on autophagy inhibition.** (A) Scheme of WT STING, cyclic dinucleotides (CDNs) binding-deficient mutant STING R232A, and autoimmunity disease mutants STING N154S or STING V155M. (B) Overexpression of STX17-myc has no effect on STING self-interaction. HEK293T cells were transfected with empty vector, STING-HA, STING-Flag, STX17-Myc as indicated. 24 h after transfection, cells were lysed and immunoprecipitated with anti-Flag antibody. Immunoblotting was performed with indicated antibodies. (C) STX17-HA interacts with STING-Flag through the region around 134–160aa of STING. HEK293T cells were transfected with empty vector, STX17-HA and Flag tagged STING truncations. 24 h after transfection, cells were lysed and immunoprecipitated with anti-Flag resin. Immunoblotting was performed with indicated antibodies. White arrows indicate designated bands of truncations of STING. (D) The cartoon of 2D STING structure. Three residues important for STX17 interaction are marked in red. (E) Representative images of LC3 puncta in cells expressing STING WT or the indicated mutants. WT MEFs, STING-KO MEFs, STING-KO MEFs stably expressing STING-HA WT, STING-HA R232A, STING-HA N154S, STING-HA V155M, or STING-HA C148A were treated with Torin 1 for 3 h and then stained with antibodies against HA and LC3. Scale bar, 10 μ m. Source data are available for this figure: SourceData FS4.

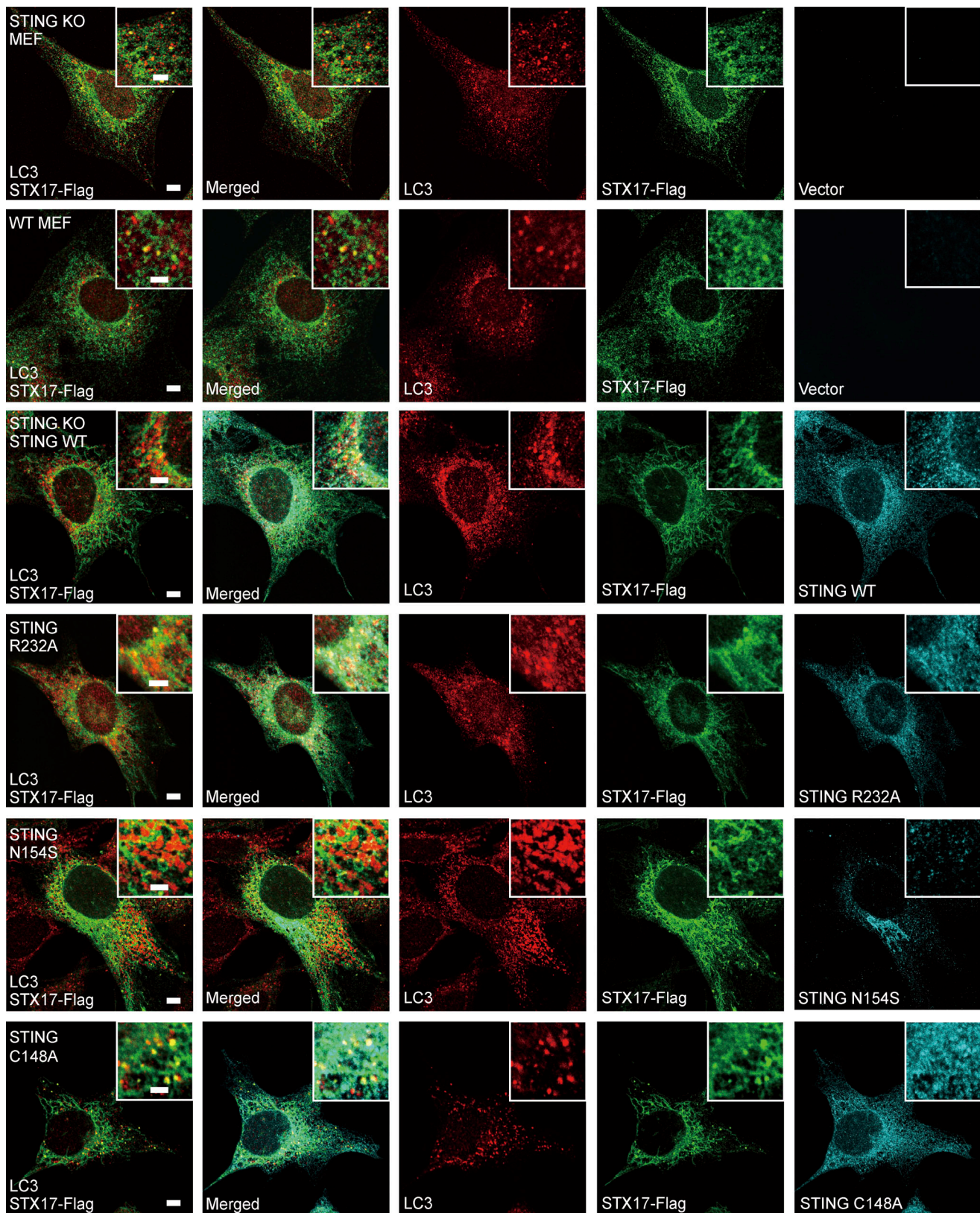


Figure S5. **Analysis of STING and STING mutants in blocking the translocation of STX17 to autophagosomes.** WT, STING-KO, and STING-KO MEFs stably expressing STX17-Flag with STING-HA WT, STING-HA R232A, STING-HA N154S, or STING-HA C148A were treated with Torin 1 for 3 h and stained with antibodies against HA, Flag and LC3. Scale bar for large images, 5 μ m; scale bar for inset images, 2.5 μ m.

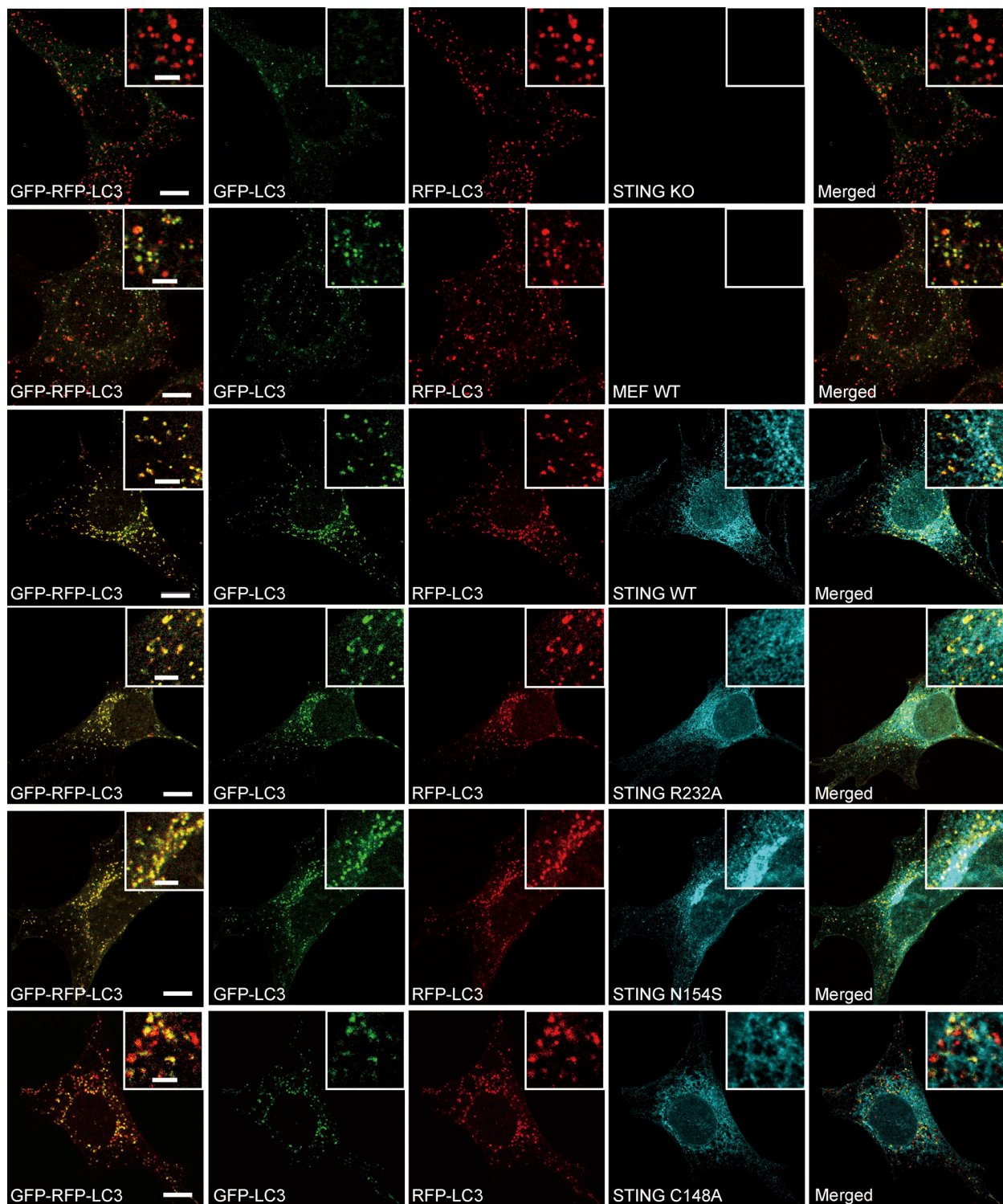


Figure S6. **Functional analysis of STING mutants in autophagosome maturation.** STING-KO MEFs reconstituted with STING-HA WT, STING-HA R232A, STING-HA N154S, STING-HA V155M, or STING-HA C148A were treated with Torin 1 for 3 h. The fluorescence of GFP-RFP-LC3 was imaged. Scale bar for large images, 10 μ m; scale bar for inset images, 2.5 μ m.